ADVANCES IN ATMOSPHERIC SCIENCES, 2021

• **Original Paper** •

Projection of the Future Changes in Tropical Cyclone Activity Affecting East Asia over the Western North Pacific Based on Multi-RegCM4 Simulations※

Jie WU[1], Xuejie GAO[*2,3], Yingmo ZHU[4], Ying SHI[5], and Filippo GIORGI[6]

[1]*School of Geography and Environmental Engineering*, *Gannan Normal University*, *Ganzhou* 341000, *China*
[2]*Climate Change Research Center*, *Institute of Atmospheric Physics*, *Chinese Academy of Sciences*, *Beijing* 100029, *China*
[3]*University of Chinese Academy of Sciences*, *Beijing* 100049, *China*
[4]*Department of Atmospheric Sciences*, *Yunnan University*, *Kunming* 650504, *China*
[5]*National Climate Center*, *China Meteorological Administration*, *Beijing* 100081, *China*
[6]*The Abdus Salam International Centre for Theoretical Physics*, *Trieste* 34100, *Italy*

(Received 21 August 2020; revised 8 December 2020; accepted 13 January 2021)

ABSTRACT

Future changes in tropical cyclone (TC) activity over the western North Pacific (WNP) under the representative concentration pathway RCP4.5 are investigated based on a set of 21st century climate change simulations over East Asia with the regional climate model RegCM4 driven by five global models. The RegCM4 reproduces the major features of the observed TC activity over the region in the present-day period of 1986–2005, although with the underestimation of the number of TC genesis and intensity. A low number of TCs making landfall over China is also simulated. By the end of the 21st century (2079–98), the annual mean frequency of TC genesis and occurrence is projected to increase over the WNP by 16% and 10%, respectively. The increase in frequency of TC occurrence is in good agreement among the simulations, with the largest increase over the ocean surrounding Taiwan Island and to the south of Japan. The TCs tend to be stronger in the future compared to the present-day period of 1986–2005, with a large increase in the frequency of strong TCs. In addition, more TCs landings are projected over most of the China coast, with an increase of ~18% over the whole Chinese territory.

Key words: regional climate model, RegCM4, tropical cyclone, western North Pacific

Citation: Wu, J., X.-J. Gao, Y. M. Zhu, Y. Shi, and F. Giorgi, 2021: Projection of the future changes in tropical cyclone activity affecting East Asia over the western North Pacific based on Multi-RegCM4 simulations. *Adv. Atmos. Sci.*, https://doi.org/10.1007/s00376-021-0286-9.

Article Highlights:

- A set of regional climate model RegCM4 simulations at 25-km grid spacing driven by five global models over East Asia was used.
- RegCM4 reproduces the major features of the observed tropical cyclone activity over the region in the present-day period.
- Tropical cyclones tend to be stronger in the future, with more tropical cyclones making landfall over China.

1. Introduction

A number of climate model studies using both global and regional climate models (GCMs and RCMs, respectively) have investigated the future changes in tropical cyclones (TCs) over different regions throughout the globe. The pioneering work of Manabe et al. (1970) used a low-resolution (~400 km) GCM, finding TC-like vortices in the simulation although with much weaker intensity than observed. In general, low-resolution GCMs can generate TC-like structures and reproduce some primary characteristics of observed TCs (Bengtsson et al., 1982, 1995; Broccoli and Manabe, 1990; Haarsma et al., 1993). However, they tend to fail in reproducing the observed intensities and internal small-scale structures of TCs because of their coarse resolution.

With the rapid development in computer technology,

※ This paper is a contribution to the special issue on the Climate Change and Variability of Tropical Cyclone Activity.

* Corresponding author: Xuejie GAO
Email: gaoxuejie@mail.iap.ac.cn

high-resolution (⩽50 km) GCMs have been developed and employed to simulate TCs and their future changes (Oouchi et al., 2006; Zhao et al., 2009; Murakami and Sugi, 2010; Reed and Jablonowski, 2011; Murakami et al., 2012a). These GCMs show better performance in representing more realistic TC features, such as convergence, heavy rainfall and high moisture at lower levels. However, they are still too expensive and difficult for use in producing multi-decadal to centennial climate change simulations. The typical horizontal resolution of models in the current phase 6 of the Coupled Model Intercomparison Project (CMIP6, Eyring et al., 2016) for long-term climate change simulations is mostly in the range of 100–200 km (https://raw.githubusercontent.com/WCRP-CMIP/CMIP6_CVs/master/src/CMIP6_source_id.html), which is still too coarse to adequately capture the TC characteristics. Thus, nested high-resolution regional climate models (RCMs) have been used in the simulation of TCs (e.g. Giorgi, 2019 and references therein).

The frequency of TCs generated in the western North Pacific (WNP) is the largest compared to any other basin. TCs, particularly those making landfall, cause great damage to East Asia (Wu et al., 2005; Zhang et al., 2009; Wang et al., 2016). Different high resolution GCMs have been used to investigate future changes in TC activity over the basin. For example, Murakami et al. (2011) used the MRI-JMA model and found a reduction in TC genesis and a decrease of the frequency of TC occurrence over the western WNP, but an increase over the southeastern WNP. Murakami et al. (2012b) also reported a future decrease in the TC frequency over the WNP. Yokoi et al. (2013) analyzed an ensemble of seven GCMs and found that the track frequency of TCs will increase over the tropical central WNP east of 140°E and be reduced over the western and northwestern parts. By applying a TC downscaling technique to six CMIP5 models, Emanuel (2013) projected increases in TC activity over the basin, which is consistent with Emanuel (2021) and Vecchi et al. (2019). Overall, these studies show substantial uncertainties about the future changes of TC activity over the region.

RCMs have also been employed for TC simulations over the WNP. Au-Yeung and Chan (2012) found that the tracks, interannual variability and climatological spatial distributions of TC occurrence over the WNP can be reproduced well by RegCM3 (Pal et al., 2007). Huang and Chan (2014) reported a better skill of RegCM3 in forecasting TC genesis and landfall over East Asian compared to the driving (nested) GCM. The simulations by Wu et al. (2014) using the GFDL-ZETAC RCM showed a weak tendency for decreases in the number of TCs, increases in the number of more intense TCs, and a weak tendency towards a poleward TC shift in the future. Phan-Van et al. (2015) reported a good performance by RegCM4 (Giorgi et al., 2012) in forecasting the distribution of TC counts and track patterns during 2012–2013. Liang et al. (2017) compared the MetUM RCM at the resolutions of 12 km and 25 km, and found improvements in the 12 km model version in simulating TC track density and radial wind structure. Based on a "RegCM3-WRF" modelling system Lok and Chan (2018a, b) projected a northward migration of TC activity in the WNP, with fewer but more intense landfalls over South China. Investigations of the RCM performances and future projections of TCs have also been carried out under the Coordinated Regional Downscaling Experiment (CORDEX, Giorgi et al., 2009) frame over different domains of the globe, including East Asia (Diro et al., 2014; Jin et al., 2016; Fuentes-Franco et al., 2017; Shen et al., 2017; Lee et al., 2019).

While much has been learned from previous studies, there are still substantial uncertainties in the projection of changes in future TC activity, especially due to their basin dependence, and further research is still needed in this area. In particular, this uncertainty is present over the WNP, where TCs are extremely important. In fact, while China suffers from huge losses of property and human life due to TC landfalls (Zhang et al., 2009), limited studies have been carried out so far in evaluating the models' performance in reproducing TC characteristics and projecting their future changes.

Recently, an unprecedented new set of 21st century climate change experiments using the regional climate model RegCM4 at 25 km grid spacing driven by 5 global models over the East Asia CORDEX domain was completed (Gao et al., 2018). This provides a good opportunity to conduct further studies on the topic of TCs in the WNP, and therefore, here we present an analysis of the projected changes in the genesis, track, intensity and landfall of TCs over the WNP based in this set of simulations.

The rest of this paper is organized as follows: Section 2 describes the model, data, TC detection and tracking method. Section 3 assesses the performance of RegCM4 in reproducing the observed TC activity. Section 4 projects future changes in TC activity and large-scale circulation. Finally, conclusions and discussion are provided in section 5.

2. Model, data and methods

2.1. *Model and data*

The regional climate model used in this study, RegCM4, was developed at the Abdus Salam International Center for Theoretical Physics (ICTP) (Giorgi et al., 2012). The simulations were performed as part of Phase II of the CORDEX-East Asia domain at 25 km grid spacing (e.g. Gutowski et al., 2016). This domain covers the whole of China, surrounding East Asia land areas and most part of the WNP basin (available at https://cordex.org/domains/region-7-east-asia/, see Fig. 1). The model was run with 18 vertical sigma layers with the top at 10 hPa. The RegCM4 includes a range of physics options; we used those selected on the basis of the work of Gao et al. (2016, 2017): the CLM land surface scheme (Oleson et al., 2008), the Emanuel convection scheme (Emanuel, 1991; Emanuel and

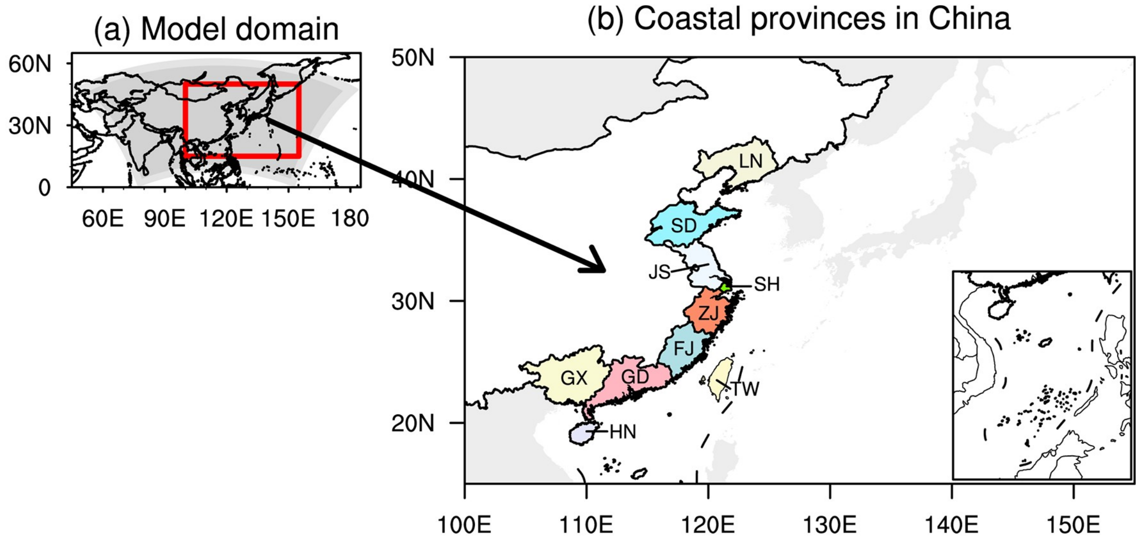

Fig. 1. (a) The CORDEX-East Asia domain (gray shading area), buffer zone (light gray shading area), and analysis zone of tropical cyclone (red rectangular). (b) Coastal provinces in China. LN, SD, JS, SH, ZJ, FJ, TW, GD, GX, and HN represent Liaoning, Shandong, Jiangsu, Shanghai, Zhejiang, Fujian, Taiwan, Guangdong, Guangxi, and Hainan, respectively.

Živković-Rothman, 1999), the NCAR Community Climate Model CCM3 atmospheric radiative transfer scheme (Kiehl et al., 1998), the planetary boundary layer scheme by Holtslag et al. (1990), the diurnal sea surface temperature (SST) scheme from Zeng and Beljaars (2005) and the SUBEX resolvable scale precipitation parameterization (Pal et al., 2000). In addition, the land cover data was updated as in Han et al. (2015) to represent a more realistic vegetation cover over China. We stress that this model configuration was not specifically selected to optimize the simulation of TCs, but was based on the more general performance assessment by Gao et al. (2016, 2017).

Initial and time evolving lateral boundary conditions are needed to drive the model, specifically for temperature, specific humidity, and wind (meridional and zonal components) at all vertical levels, as well as surface pressure and SST. These were interpolated from five different CMIP5 (Taylor et al., 2012) GCM outputs. The lateral boundary conditions scheme was carried out with an exponential relaxation technique (Giorgi et al., 1993), with a lateral buffer zone width of 12 grid points. The lateral boundary conditions and the prescribed SST were updated every 6 hours.

The five driving CMIP5 GCMs are CSIRO-Mk3.6.0 (Rotstayn et al., 2010), EC-EARTH (Hazeleger et al., 2010), HadGEM2-ES (Collins et al., 2011), MPI-ESM-MR (Jungclaus et al., 2013; Stevens et al., 2013) and NorESM1-M (Bentsen et al., 2013; Iversen et al., 2013). The horizontal resolutions of their atmospheric components are $1.875° \times 1.875°$, $1.125° \times 1.125°$, $1.875° \times 1.25°$, $1.875° \times 1.875°$ and $2.5° \times 1.875°$ (longitude × latitude), respectively. These models were selected because of data availability, their relatively high resolution within the CMIP5 model ensemble, and their good performance in simulating present day temperature and precipitation over China [with spatial correlation coefficients and standardized deviations in general better than many other models, as reported by Jiang et al. (2016)]. The five simulations are hereafter referred to as CdR, EdR, HdR, MdR and NdR, respectively, following the above GCM names. The simulations cover the present-day period of 1968–2005 with observed greenhouse gas (GHG) concentrations and 2006–98 for the future under the representative concentration pathway RCP4.5 (Moss et al., 2010). GHG concentrations are updated each year throughout the simulation period.

The reference period used here is 1986–2005 (20 years), and the term "change" refers to the difference between a future and reference period (present-day). The WNP region is considered to be 15°–50°N and 100°–155°E (Fig. 1), which is smaller than that previously used due to the size of the recommended CORDEX model domain (e.g. Murakami et al., 2011; Au-Yeung and Chan, 2012; Lee et al., 2019). The model results were interpolated bilinearly onto the same grid with resolution of $0.25° \times 0.25°$. The ensemble mean of the 5 runs was derived using an equally weighted ensemble averaging method and is indicated by ensR.

Six-hourly best track data of observed TCs for model validation were obtained from the International Best Track Archive for Climate Stewardship (IBTrACS v03r10) (Knapp et al., 2010) for the period of 1986–2005. The dataset provides information from different regional TC observational centers, containing 6-hourly storm positions, maximum wind speed, minimum central pressure, etc. Several collections are available in the dataset. We used the one from the World Meteorological Organization (WMO) sanctioned forecast agencies (IBTrACS_wmo). TCs that developed into extratropical cyclones were removed from the tracks in our study.

The steering flow, which predominantly regulates the variation in TC tracks and landfall positions (Gray, 1979; Chan, 2005; Li et al., 2017), is defined as the average flow from 300 hPa to 850 hPa. An observational estimate was obtained from the ERA-Interim dataset (Dee et al., 2011) with 1.5° × 1.5° resolution from June to September during 1986–2005. The steering flow from RegCM4 was interpolated onto the 1.5° × 1.5° grid using a mass conservation method.

2.2. *TC detection and tracking methods*

Different methods for TC detection and tracking examined have only relatively minor differences among each other. The software of TSTORMS (Detection and Diagnosis of Tropical Storms in High-Resolution Atmospheric Models) provided by Geophysical Fluid Dynamics Laboratory (https://www.gfdl.noaa.gov/tstorms/) is employed in the present study. The method uses the basin-, time-, and model-dependent vorticity as proposed by Camargo and Zebiak (2002). In this method, a vorticity threshold is defined as twice the standard deviation of the 850 hPa relative vorticity in the analysis area. The values of the vorticity and temperature anomaly criteria used for the present-day period of 1986–2005 and future climate simulations are listed in Table 1. Note that, because the maximum wind threshold correlates closely with the spatial (Walsh et al., 2007) and temporal (Kruk et al., 2010) resolution, it is not considered here as a detection criterion.

Preliminary analysis of the sensitivity of TC genesis number to the different detection criteria showed that it is most sensitive to the lifespan, to a lesser extent to the warm core, and least to the 850 hPa relative vorticity. Larger values of the warm core criteria decrease the number of weak TCs, but show little change for the intense ones. Based on the 6-hourly data, the TC detection procedure can be summarized as follows:

- The 850 hPa relative vorticity maximum in a centered 20 × 20 grid box exceeds the vorticity threshold.
- The local sea level pressure (SLP) minimum is considered as the TC center, and the distance of this TC center from the vorticity maximum must not exceed 2° longitude or latitude.
- The local maximum temperature averaged between 200 hPa and 500 hPa is defined as the warm core center, which should be within a radius of 2° longitude or latitude from the TC center. The temperature of warm core minus the averaged surrounding temperature must exceed the vertically integrated temperature anomaly threshold.
- The TC center at genesis should be over warm ocean points where the SST is higher than 26°C.

Table 1. Thresholds of 850 hPa relative vorticity (10^{-6} s^{-1}) and warm core temperature (°C) for detecting TCs.

Time period	Simulations	Relative vorticity (10^{-6} s^{-1})	Warm core (°C)
1986–2005	CdR	5.87	1
	EdR	5.78	1
	HdR	6.80	1
	MdR	6.50	1
	NdR	5.76	1
2079–98	CdR	6.15	1
	EdR	5.94	1
	HdR	6.89	1
	MdR	6.82	1
	NdR	5.83	1

We selected the potential TC centers satisfying the above detection criteria, and then a trajectory analysis was performed to link the TC centers in time for a given track using the following procedure:

1) For each detected TC point, a check was performed to see if there were TCs during the following 6-hour period within a distance of 400 km.

2) If several candidates exist, the closest TC was considered as belonging to the same track as the initial one. If more than one possibility is found, the ones which were to the west and poleward of the current location were preferred.

3) To qualify as a TC trajectory, a TC needed to last for at least 1 day.

The TC positions were counted for each 2° × 2° grid over the region, with the total count for each grid defined as the frequency (number) of genesis or occurrence.

The intensity of TCs was categorized following the China National Standard of GB/T19201–2006 as employed in the operational services at the China Meteorological Administration (http://tcdata.typhoon.org.cn/doc/TC_std.pdf). Namely, they are classified as tropical depression (TD), tropical storm (TS), strong tropical storm (STS), typhoon (TY), strong typhoon (STY), and super typhoon (SuperTY), by use of the thresholds for each category presented in Table 2. Note that the maximum wind speed during the entire life-time of a TC is used to identify the category of a specific TC, without considering intensities in different periods of its life cycle. In addition, the standard lower wind limit of 10.8 m s^{-1} to define a tropical depression is removed due to the underestimation of local wind speed in

Table 2. Categories of tropical cyclones used in the study[a].

Category	Winds (m s^{-1})
Tropical Depression (TD)	<17.1
Tropical Storm (TS)	17.2–24.4
Strong Tropical Storm (STS)	24.5–32.6
Typhoon (TY)	32.7–41.4
Strong Typhoon (STY)	41.5–50.9
Super Typhoon (SuperTY)	⩾51.0

[a]: Following the China National Standard of GB/T19201–2006 as employed in the operational services in China Meteorological Administration.

the simulations related to the relatively coarse model resolution (e.g. Jin et al., 2016).

In the Saffir-Simpson hurricane wind scale, the TC is classified into tropical depression (<17 m s^{-1}), tropical storm (17–33 m s^{-1}), category 1 (33–43 m s^{-1}), category 2 (43–49 m s^{-1}), category 3 (50–58 m s^{-1}), category 4 (58–70 m s^{-1}), and category 5 (>70 m s^{-1}), respectively. Thus TY here is close to category 1, STY is close to category 2, and SuperTY includes the categories 3–5 of the Saffir-Simpson scale.

3. Validation of the simulated present day TC activity

3.1. *Genesis, occurrence frequency, and tracks*

The distributions of the mean TC genesis locations from the observation and simulations for the present-day period (1986–2005) are presented in Fig. 2. The TC genesis number is largest at lower latitudes between 15°N and 25°N in the southern part of the analysis region. The mean annual total number and interannual variability (as measured by the standard deviation) in the observations are 23.9 yr^{-1} and 4.3 yr^{-1}, respectively.

The pattern of TC genesis is generally well captured by the simulations (Figs. 2b–g), with a spatial correlation coefficient ranging from 0.42 (NdR) to 0.58 (ensR). The regional mean genesis frequency in the simulations ranges from 14.0 yr^{-1} to 30.0 yr^{-1}. Note that domain-wide nudging from the driving GCMs is not applied in the simulations, however, the influence of lateral and lower boundary conditions is reflected by the large range of TC numbers across ensemble members (e.g. Wu and Gao, 2020).

The value for ensR is 23.0 yr^{-1}, quite close to that observed. As shown in Fig. 2h, a mixture of positive and negative biases is found over the region in ensR, with the regional mean bias as −0.9 yr^{-1}. For the individual simulations, greater overestimation is found for MdR, more pronounced north of 20°N, and to a less extent CdR (Figs. 2e, 2b). Close values are found for EdR and HdR. The underestimation is largest for NdR, with a regional mean value of 14.0 yr^{-1}, less than half of the largest one (MdR: 30.0 yr^{-1}). Therefore, the inter-model range in simulated TC occurrences is also quite pronounced spatially. Concerning the interannual variability in TC occurrences, the values in the individual simulations fall within the range of 4.0 yr^{-1} (NdR) to 5.9 yr^{-1} (CdR), mostly greater than that observed (4.3 yr^{-1}), with the mean of the simulations being 5.2 yr^{-1}. The interannual variability is evidently related to the total number of events, since the ratio of standard deviation over mean in ensR is 0.23, slightly larger than that in the observations (0.18).

Figure 3a compares the observed and simulated annual cycle of the monthly mean TC genesis. The observed genesis frequency shows distinct seasonal variations, with a maximum (5.1 mon^{-1}) in the late summer (August) and a minimum (0.1 mon^{-1}) in late winter (February). The annual cycle is in general reproduced by the simulations, with the largest numbers during the warm season and smallest numbers during the cold season. The underestimation for NdR is evident in all months, and with HdR shifting the maximum to September. The worst performance is found by CdR, which simulates two peaks, in June and October. MdR also simulates two peaks, in August and October, and excessive numbers are simulated in May–June and October–December, resulting in a longer TC season than observed. EdR overestimates the frequency during May–June and November–December. Taken together as an ensemble, these simulations result in an overall close frequency of genesis during the year to that observed, and a peak shift to September in ensR.

The occurrence frequency from the observations and simulations is provided in Fig. 4. In the observations, the frequency is largest in the south between 15°–20°N and west of 135°E, and extends to the northeast over the ocean. Three maxima are found, located in the South China Sea, northeast to Taiwan Island, and the tropical sea east of the Philippines, respectively (Fig. 4a). The regional mean observed occurrence frequency is 1.18 yr^{-1}.

Similar to the TC genesis, the spatial pattern of the occurrence frequency is generally captured by the simulations, with correlation coefficients in the range of 0.69–0.87. A general underestimation of the frequency is found in all simulations with a regional mean value ranging from 0.38 yr^{-1} to 0.82 yr^{-1}. For CdR, with the relatively low correlation coefficient (0.70), the underestimation is most pronounced over the sea along the continental coast (Fig. 4b). EdR, HdR, and MdR perform better, with correlations greater than 0.80 (Figs. 4c–e). Consistent with the underestimation of genesis frequency (Fig. 2f), an overall underestimation in the occurrence frequency is found in NdR (Fig. 4f) over the region, with the regional mean value as less than half of the observed and the lowest correlation coefficient (0.69).

The correlation coefficient of ensR for the occurrence frequency is 0.84, slightly less than the largest individual one (EdR). Regional mean value of the occurrence frequency for ensR is 0.67 yr^{-1}, ~43% less than the observed, mostly contributed by a zone with large negative bias (>1.5 yr^{-1}) from the South China Sea extending northeastward to south Japan (Fig. 4h). The underestimation of occurrence frequency, along with the slightly underestimated genesis frequency noted in Fig. 2, imply that the simulated storms have a shorter lifetime than observed. Note it is difficult to unambiguously identify the cause of the model biases, as it may depend on many factors derived from either the GCM forcing or inherent in the model. An important one is the selection of the cumulus convection scheme. For example, Diro et al. (2014) showed that the use of the Emanuel scheme in RegCM4 tends to produce relatively high numbers of TCs over the Eastern Equatorial Pacific and Western Atlantic basins, and therefore this may be a contributing factor also in our simulations.

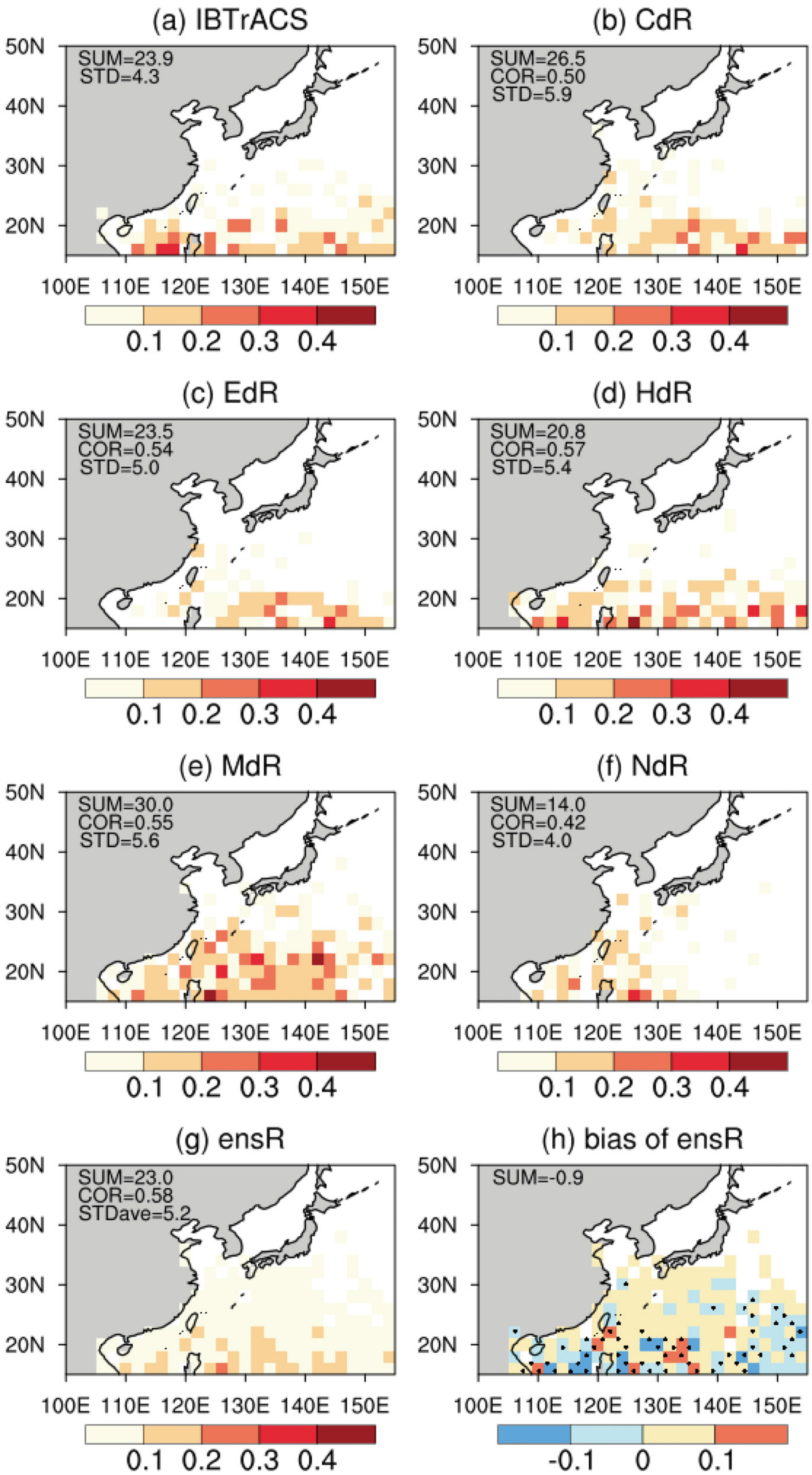

Fig. 2. Annual mean TC genesis frequency (number per 2° × 2° square per year) over the western North Pacific (WNP) in the present-day period (1986–2005) from (a) IBTrACS, (b) CdR, (c) EdR, (d) HdR, (e) MdR, (f) NdR, and (g) ensR, and (h) the bias of ensR. Regional sums, the correlation coefficients with observation, and the interannual variabilities are provided in the upper left corner of the panels. Dots in (h) indicate grid points where at least four out of five simulations agree on the sign of the bias.

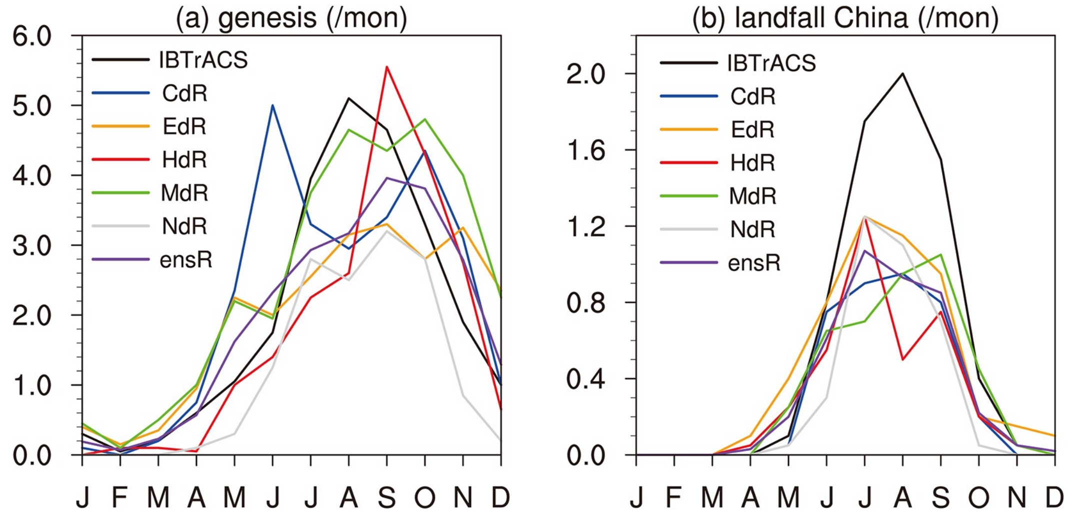

Fig. 3. Annual cycle of regional mean TC frequency (number per month) of (a) genesis over the WNP and (b) landfall in China in the present-day period of 1986–2005.

Figure 5 presents the TC tracks from the observations and simulations. The simulated TC tracks show general agreement with the observations, characterized by a motion towards the west first and then followed by a prevailing northwestward track. The track density in the simulations also agrees well with the observed except for NdR, which is characterized by much lower frequencies to the north and east of 135°E (Fig. 5f). An underestimation of the TC intensity is evident from the figure, with fewer STY and SuperTY compared to the observations (see more discussion below).

3.2. *Intensity, landfalls and large-scale circulation*

The percentage of the total number of TC for different duration, grade, and minimum SLP are presented in Figs. 6a–c. In the observations, the duration shows a peak of 6–8 d (27%), followed by the 4–6 d interval (24%), with the percentage for longer than 12 d being 9%. Only 2% of TCs fall in the length interval of less than 2 d. The distribution of the TC duration shows a similar behavior across simulations, but with a tendency towards shorter life cycles, e.g. over ~36% and ~24% of TCs lasting less than 2 d and within 2–4 d, respectively. Conversely, the percentage for TCs lasting more than 10 d is only ~5%, much less than observed (21%). As already mentioned, the shorter duration of TCs leads to the general underestimation of the occurrence frequency shown in Fig. 4, even though a close number of genesis events are simulated (Fig. 2).

For the TC grades (Fig. 6b), the largest portion (28%) of TCs is classified as TY in the observations, followed by TS (23%), STS (20%), STY (18%), SuperTY (11%), and TD (0.2%). The distributions of TC grades in the individual simulations show consistency with that observed, but with larger portions for TS (~31%) and STS (~39%), an overestimation of TD (~5%), and underestimation of TY (~21%), STY and SuperTY (<~5%). Therefore, the models tend to underestimate especially the strongest events.

The minimum SLP is another important indicator of the TC intensity. In the observation dataset, over half of the TCs fall in categories with minimum SLP lower than 970 hPa, and fewer than 4% are in the category greater than 1000 hPa (Fig. 6c). On the other hand, the values of minimum SLP for the simulated TCs are mostly greater than 970 hPa, with the ones in the category of 950–970 hPa found only in HdR and MdR. In summary, similarly to previous studies, the intensity of TCs in the model simulations tends to be weaker than observed. This is not unexpected, since very high resolution, up to a few km, may be needed to simulate intense TCs (e.g. Gentry and Lackmann, 2010; Murakami and Sugi, 2010).

Preliminary analysis of the driving GCMs show a dominant cold SST bias and a general underestimation of the vorticity at 850 hPa over the region (Fig. 7). This may contribute to generating short life cycles and reduced intensity of the TCs simulated in RegCM4. However, further analysis and experiments are needed to demonstrate this and ultimately improve the model performances. This also emphasizes the importance of the selection of the driving GCMs and/or the use of bias correction for the SST before these are input into the RCMs.

Figure 3b presents the annual cycle of the observed and simulated monthly mean number of TCs making landfall over China during 1986–2005. The observed landfall number shows distinct seasonal variations, with a maximum found in August (2 mon^{-1}), consistent to the genesis frequency (Fig. 3a). The simulations capture the annual cycle well, except for the presence of two peaks in HdR (July and September). The landfall numbers in CdR reach a maximum in August, same as in the observations, but the peaks are in July for EdR, HdR, NdR and consequently ensR.

Figure 8 compares observed and simulated histograms of annual mean number of landfall TCs in Chinese coastal provinces (including also Guangxi Autonomous Region and Shanghai City, with the names and locations provided in Fig. 1b) and the entirety of China coastal areas. Note that

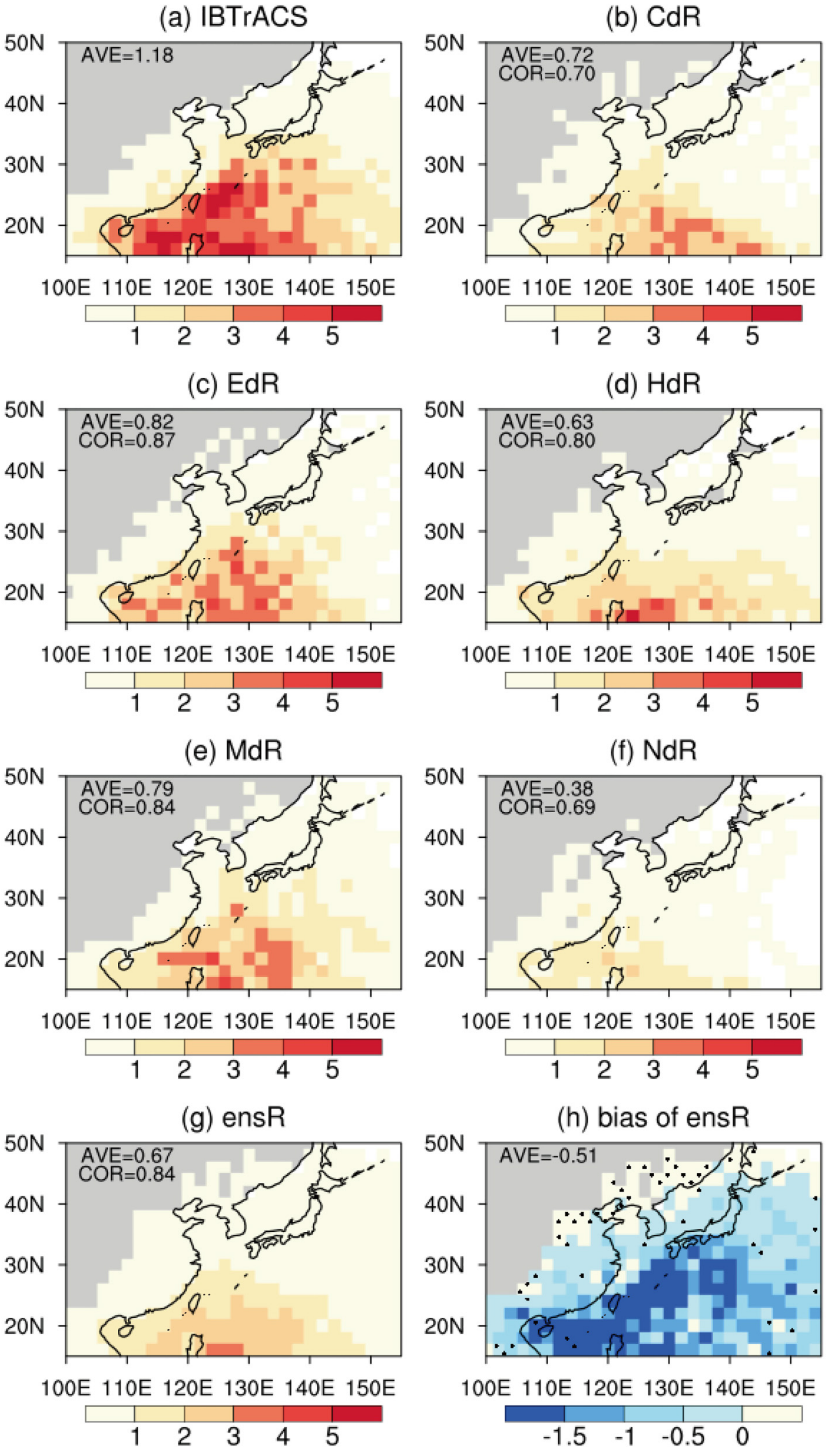

Fig. 4. Annual mean TC occurrence frequency (number per 2° × 2° square per year) over the WNP in the present-day period of 1986–2005 from (a) IBTrACS, (b) CdR, (c) EdR, (d) HdR, (e) MdR, (f) NdR and (g) ensR in the present-day period of 1986–2005, and (h) the bias of ensR. Regional means and the correlation coefficients with observation are provided in the upper left corner of the panels. The dots in (h) indicate grid points where at least four out of five simulations agree on the sign of the bias.

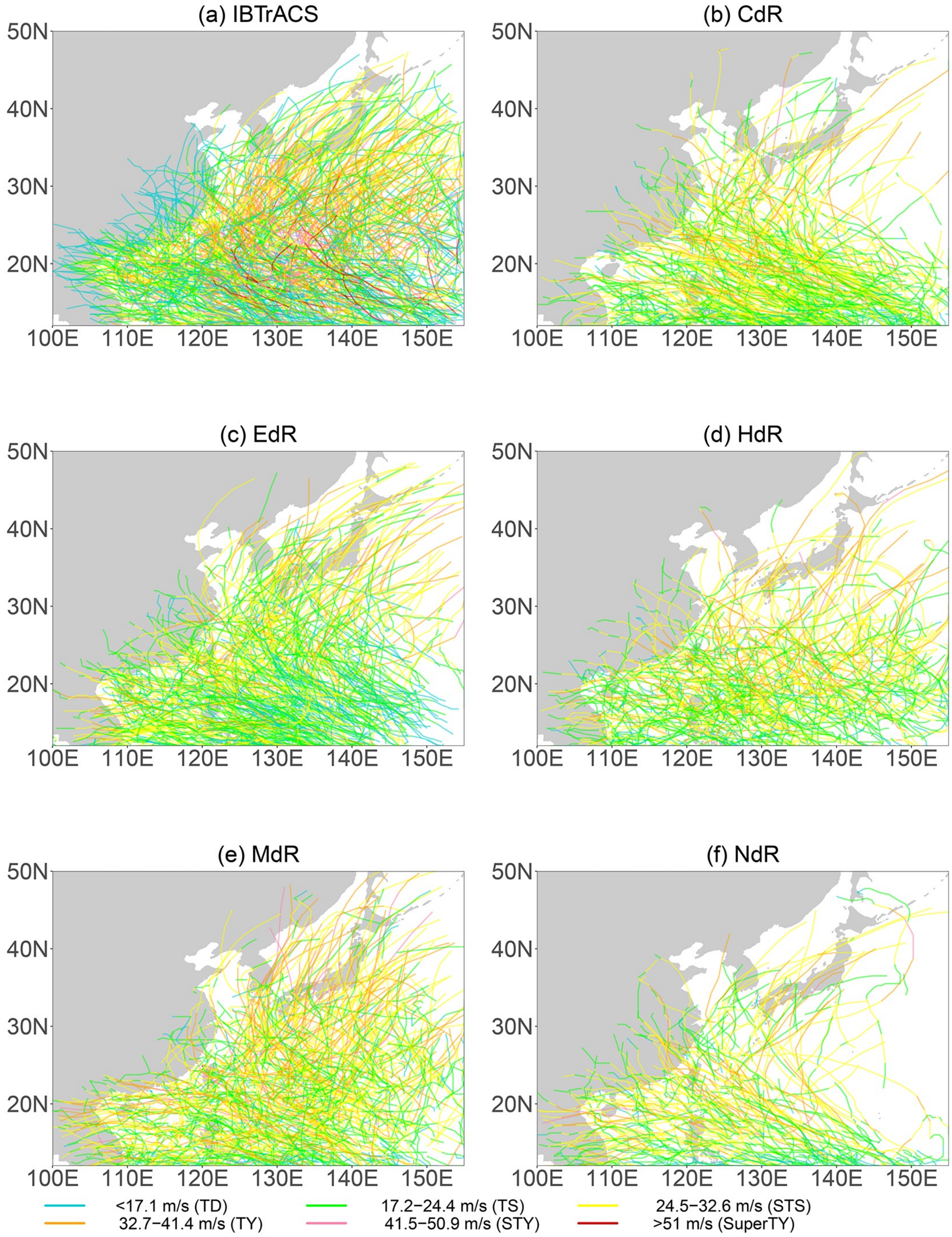

Fig. 5. TC tracks over the WNP from (a) IBTrACS, (b) CdR, (c) EdR, (d) HdR, (e) MdR and (f) NdR in the present-day period of 1986–2005. TC tracks are color coded based on the intensities of TCs as shown in Table 2 (TD: tropical depression, TS: tropical storm, STS: strong tropical storm, TY: typhoon, STY: strong typhoon, and SuperTY: super typhoon).

the total number of landfalls in China can be smaller than the sum of the provinces because the former is counted only once per TC, however in the latter case a TC may actually affect more than one province, and thus be counted more than once (Chan and Xu, 2009; Huang and Chan, 2014).

The observed TCs tend to make landfall in the southern provinces at lower latitudes more than observed (Fig. 8). Guangdong experiences the most frequent TC landfalls (2.9 yr^{-1}) followed by Guangxi (1.5 yr^{-1}), Fujian and Taiwan (both 1.4 yr^{-1}). The distribution of landfall numbers is captured by the individual simulations and ensR, but a general underestimation over most of the provinces and the whole of China is found. The underestimation is largest in Guangdong followed by Guangxi, with the numbers of landfalls in ensR being about half of the observed. The landfall number for the whole of China is 6.7 yr^{-1} in the observations and

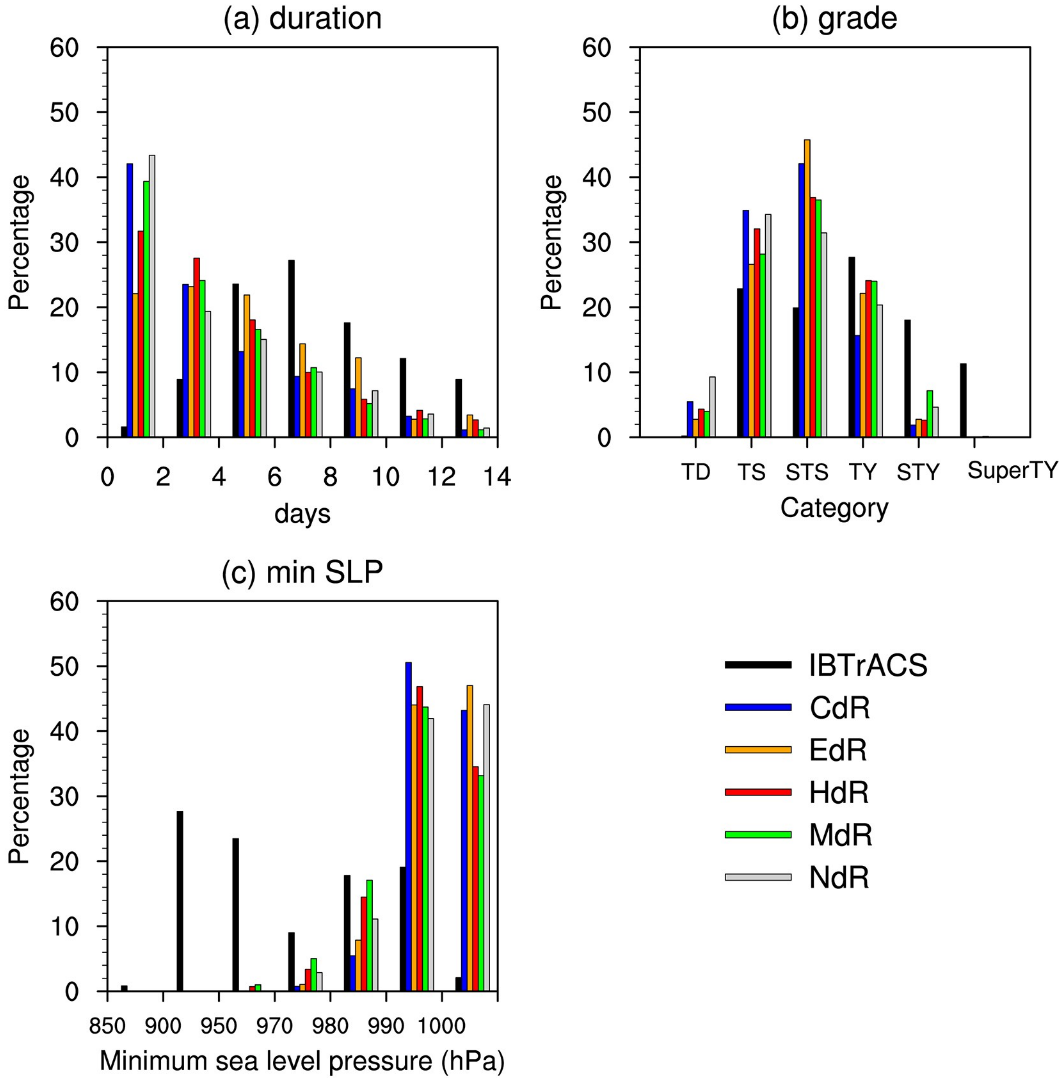

Fig. 6. Histograms of the percentages (%) of (a) TC duration, (b) different grades of TC and (c) minimum SLP from IBTrACS, the individual simulations, and ensR over the WNP in the present-day period of 1986–2005.

4.0 yr^{-1} in ensR, i.e. a bias of −2.7 yr^{-1} (~ −40%). This underestimate is evidently due to the underestimation of the occurrence frequency (Fig. 4h), and the shorter TC duration (Fig. 6a).

While the large-scale circulations influence the TC genesis and development, the environmental steering flow predominantly governs the TC tracks and landfall positions. Figures 9a and 9b show the spatial distribution of the steering flow during the TC season (June to September) from the ERA-Interim reanalysis and the bias of the ensR. The observed steering flow shows an anti-cyclonic circulation, which is in fact the western Pacific subtropical high, with larger westerly wind at high latitudes (the westerlies). Compared to the observations, the bias pattern in the simulations shows a cyclonic circulation over most of the WNP, with a dominant onshore flow into the Chinese mainland north of 25°N, which is favorable for the landfall of TCs. Thus, although there is an underestimation of the occurrence frequency (Fig. 4h), the landfall numbers in the northern provinces are still close to those observed (Fig. 8). Meanwhile an offshore bias exists south of 25°N, leading to a large underestimation of landfalls in Guangdong and Guangxi.

4. Projection of TC activity at the end of the 21st century

4.1. *Genesis frequency*

Projected changes in the TC genesis frequency by the end of the 21st century (2079–98) from the individual simulations and ensR are presented in Fig. 10. In general, the change patterns show a mixture of increases and decreases. However, the increases are predominant in all of the five simulations. The regional mean values of the increase are largest for CdR, 6.7 yr^{-1} (25%), followed by EdR and MdR, with identical values of 4.7 yr^{-1} (20%) and 4.7 yr^{-1} (16%), respectively, HdR, 1.4 yr^{-1} (7%), and NdR, 1.1 yr^{-1} (8%).

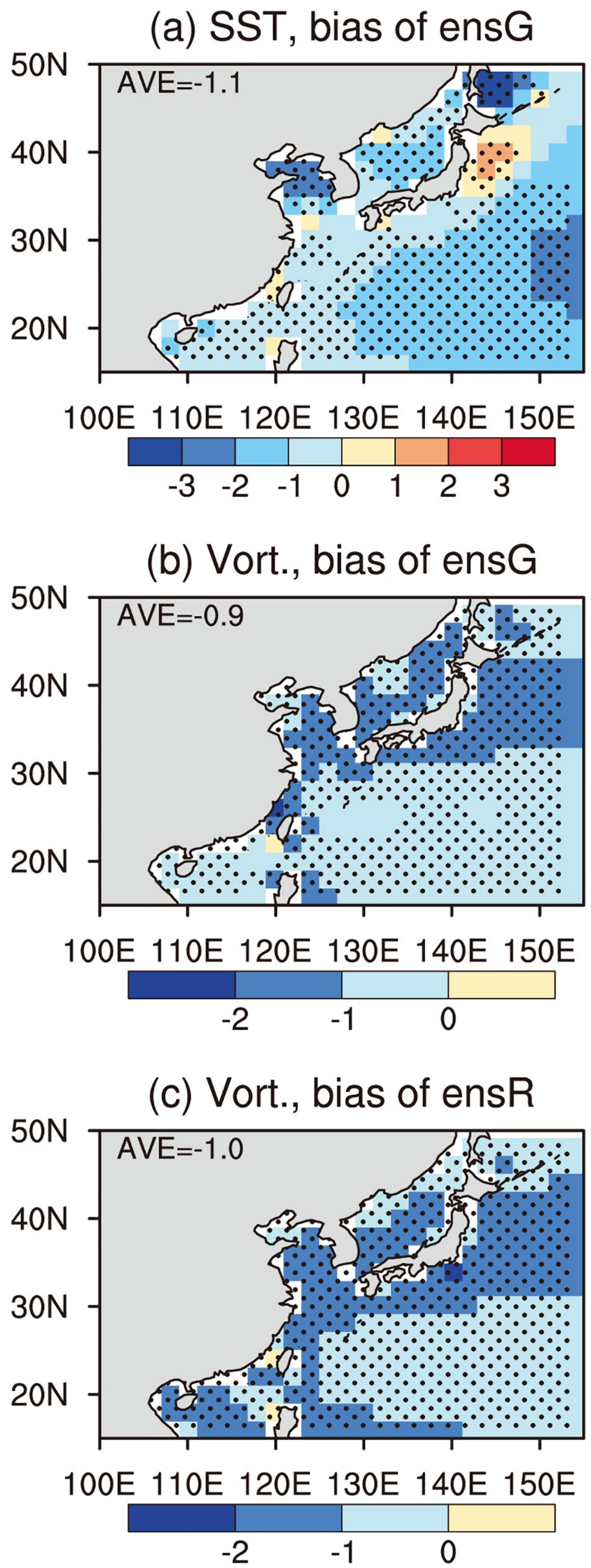

Fig. 7. Biases of sea surface temperature (SST) (a, °C), relative vorticity at 850 hPa (b, 10^{-5} s^{-1}) from ensG, and (c) the bias of relative vorticity at 850 hPa from ensR averaged from June to September in the present-day period of 1986–2005. The dots in (c) indicate grid points where at least four out of five simulations agree on the sign of the bias.

The increase of TC genesis frequency is dominant in ensR over the region, although with poor agreement at the individual grid box level among the simulations (Fig. 10f). The regional mean increase of TC genesis in ensR is 3.7 yr^{-1} (16%). The projected increase of TC genesis frequency may be due to the dominant favorable environment for TC formation, such as the increases of relative vorticity at 850 hPa, relative humidity at 700 hPa, etc. (figure not shown for brevity). However, further diagnostics and especially the design of new experiments are needed to better investigate the underlying mechanism.

Figure 11a compares the annual cycle of monthly mean TC genesis number between the present-day period of 1986–2005 and the end of the 21st century. The general characteristics of the seasonal evolution of the TC genesis remains unchanged, with a pronounced late summer maximum. General increases are found in most months except May and October (see also Fig. 11b). The increase is largest in August (1.33 mon^{-1}), followed by July (1.03 mon^{-1}) and September (0.62 mon^{-1}), with best cross-simulation agreement in August and September. The percentage increases are largest in January (47%) and August (42%), and substantial values are also found during February, June, July and September (16%–35%).

4.2. *Occurrence frequency and causes*

The future changes of TC occurrence frequency for the individual simulations and ensR are shown in Fig. 12. The changes show a general increase in four out of the five simulations, being most pronounced for CdR (regional mean of 0.20 yr^{-1}, or 28%). A mixture of negative-positive change is found in HdR, MdR, and NdR, with the regional mean showing increases ranging from 0.02–0.11 yr^{-1} (3%–16%). A broad decrease in the south and increase in the northeast is found for EdR, with the regional mean showing a decrease by 0.07 yr^{-1} (−9%). A general increase is found in ensR (Fig. 12f), more pronounced (>0.6 yr^{-1}) over the ocean east of Taiwan, south of Japan, and the region around (20°N, 140°E). The change over the tropical ocean at low latitudes shows larger areas of decrease, indicating a slight northward shift of the TC tracks in the future. Furthermore, a tendency for TCs penetrating further inland is evident. The increases are in good agreement among the simulations, with a regional mean of 0.06 yr^{-1} (10%).

Concerning the causes for the future changes in the TC occurrence frequency, we decompose it into three components, i.e. changes in TC genesis frequency, occurrence frequency/track, and the nonlinear effect, as suggested by Murakami et al. (2013a, b) and Yokoi et al. (2013). To be more specific, the change in the region A [δTCF(A)] is decomposed as:

$$\delta \mathrm{TCF}(A) = \iint_A \delta g(A_0)\, \bar{p}(A|A_0)\, \mathrm{d}A_0 + \iint_A \bar{g}(A_0) \times \delta p(A|A_0)\, \mathrm{d}A_0 + \iint_A \delta g(A_0)\, \delta p(A|A_0)\, \mathrm{d}A_0\,,$$

where δ represents the future change (relative to the present-

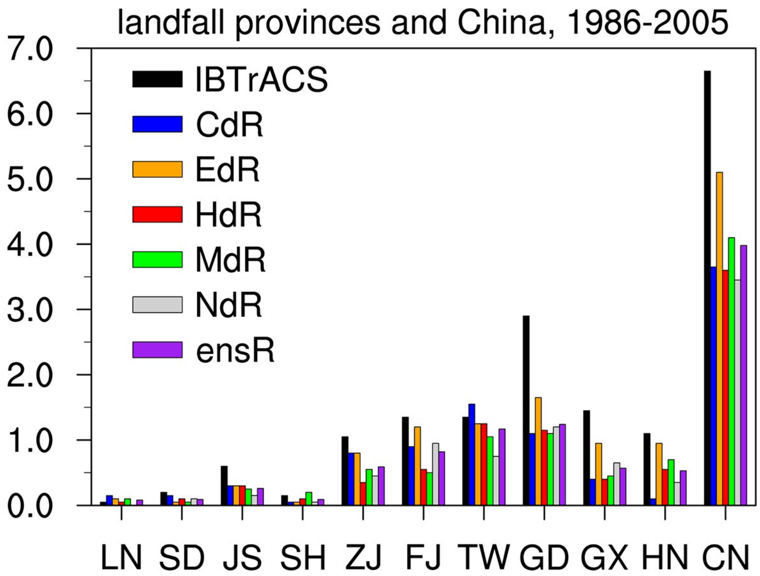

Fig. 8. Histograms of annual mean number of landfall TCs (number per year) in the coastal provinces and entirety of China from the observation and simulations in the present-day period of 1986–2005.

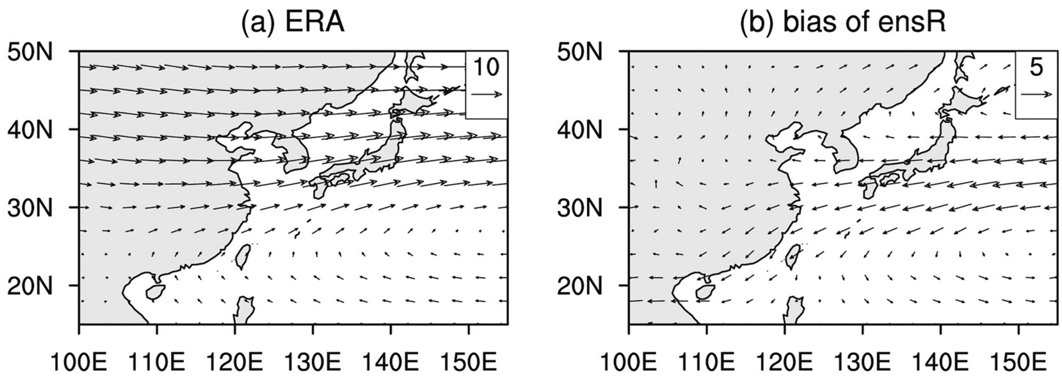

Fig. 9. Steering flow (vector; m s^{-1}) averaged from June to September from (a) ERA-Interim and (b) biases of ensR in the present-day period of 1986–2005.

day period of 1986–2005), the bar indicates present day conditions, TCF(A) the total occurrence frequency over the region A, $g(A_0)$ the genesis frequency over each grid cell, $p(A|A_0)$ the probability that a TC generated in the grid cell A_0 travels to the region A, respectively. $\iint_A \delta g(A_0) \times \bar{p}(A|A_0)\,\mathrm{d}A_0$ represents the future change in TCF due to TC genesis; $\iint_A \bar{g}(A_0)\delta p(A|A_0)\,\mathrm{d}A_0$ represents the contributions from TC tracks to TCF; and $\iint_A \delta g(A_0)\delta p(A|A_0)\,\mathrm{d}A_0$ represents the non-linear contribution of the simultaneous changes of TC genesis and track distribution. A_0 represents each 2° × 2° grid cell and A is the entire analysis domain.

Future changes due to the three factors are shown in Fig. 13. The contribution from the genesis is found only over portions of the region, showing a decrease along the eastern China coast, the South China Sea, and east of the Philippines and an increase further east (Fig. 13a). Thus the prevailing increase of the genesis frequency over the region (Fig. 10f) does not provide a major contribution to the occurrence frequency. The factor of the preferable track change shows a negative contribution over the region west of 130ºE, but mostly positive to the east (Fig. 13b), while a predominant increase contribution is found for the nonlinear term throughout the region (Fig. 13c), which is evidently the main contributor to the change in TC occurrence. Changes in the preferable track contributes also to the large frequency increase over the eastern part of the region and northeast of Taiwan, while the decreases in the lower latitudes are mostly due to the changes in genesis and preferable track.

4.3. *Intensity, landfalls and large-scale circulation*

Percentages of TC duration, grades and minimum SLP for ensR and the spread of the simulations for the present-day period of 1986–2005 and at the end of the century periods are presented in Fig. 14. The duration of the TCs shows little change in the future (Fig. 14a), with a mix of positive and negative change found throughout the distribution. For example, an increase from 36% to 39% is found for the dura-

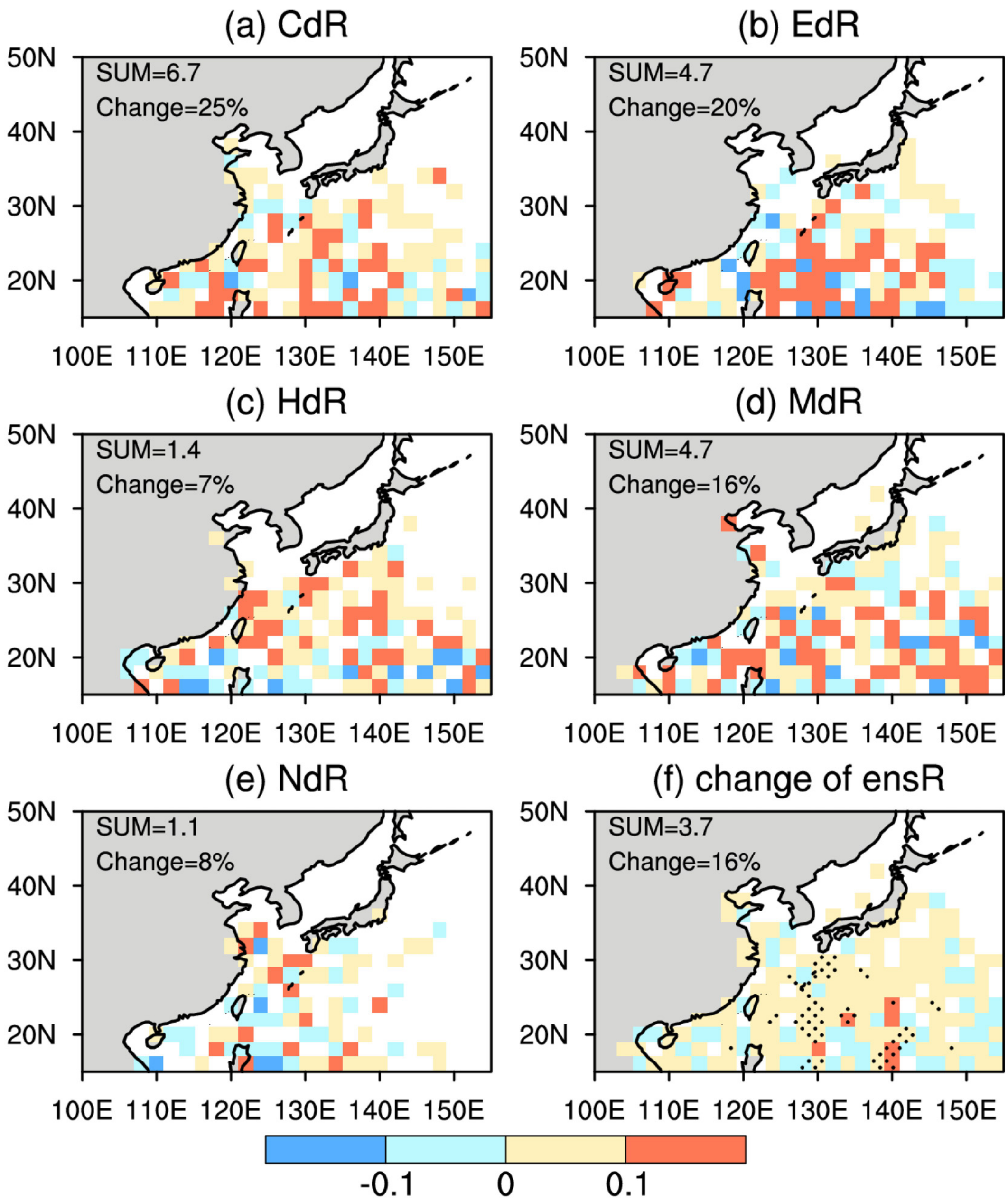

Fig. 10. Projected annual mean changes of genesis frequency (number per 2° × 2° square per year) from (a) CdR, (b) EdR, (e) HdR, (d) MdR, (e) NdR and (f) ensR over the WNP in the end of 21st century (2079–98, in relative to 1986–2005). Regional sums and the percentage of the changes are provided in the upper left corner of the panels. The dot in (f) indicates at least 4 out of 5 models agree on the sign of change.

tion of 0–2 d, and a decrease from 17% to 14% for durations of 4–6 d. The spread is in general small among the simulations.

For the grades (Fig. 14b), we find a decrease in the low to mid-level TS and STS categories and an increase in the high end categories TY and STY, thus illustrating a distribution shift towards more intense tropical storms. In particular, the percentage of STY is almost doubled in the future compared to the present-day period (from 4% to 7%), indicating more intense TCs in the future. This result is confirmed by an increase in the percentage of minimum SLP in the categories less than 990 hPa and a decrease in the category higher than 990 hPa (Fig. 14c). Specifically, the percentage of TCs with minimum SLP less than 980 hPa increases from ~3% in the present-day period to ~5% in the future (~57% more), and with SLP less than 990 hPa from 14% for the present-day period to about 19% for the future (~31% more).

The number of TCs landing over China and its coastal provinces, together with the spread of the simulations, in the present-day period of 1986–2005 and at the end of the 21st century time-slices are shown in Fig. 15a. The number of

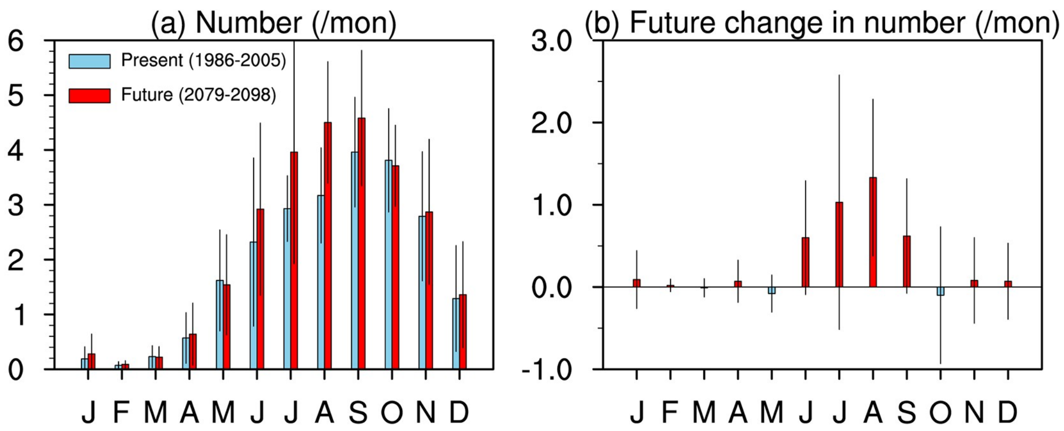

Fig. 11. Annual cycle of regional averaged TC (a) genesis frequency (number per month) during the present-day period of 1986–2005 (blue bars) and at the end of the 21st century (red bars) from ensR and (b) future change (number per month) over the WNP. The vertical lines indicate one standard deviation of the five simulations.

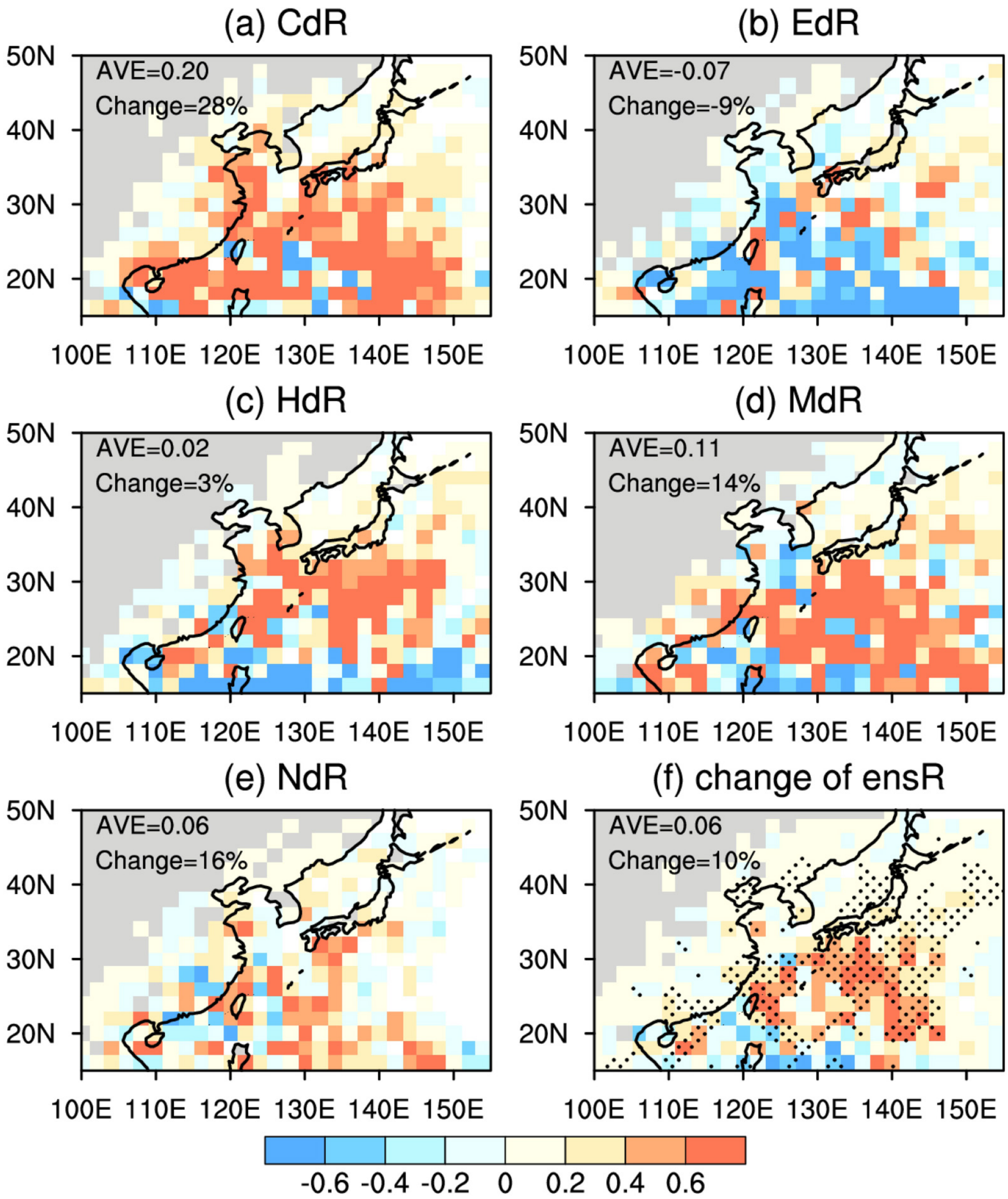

Fig. 12. Same as Fig. 10, but for occurrence frequency.

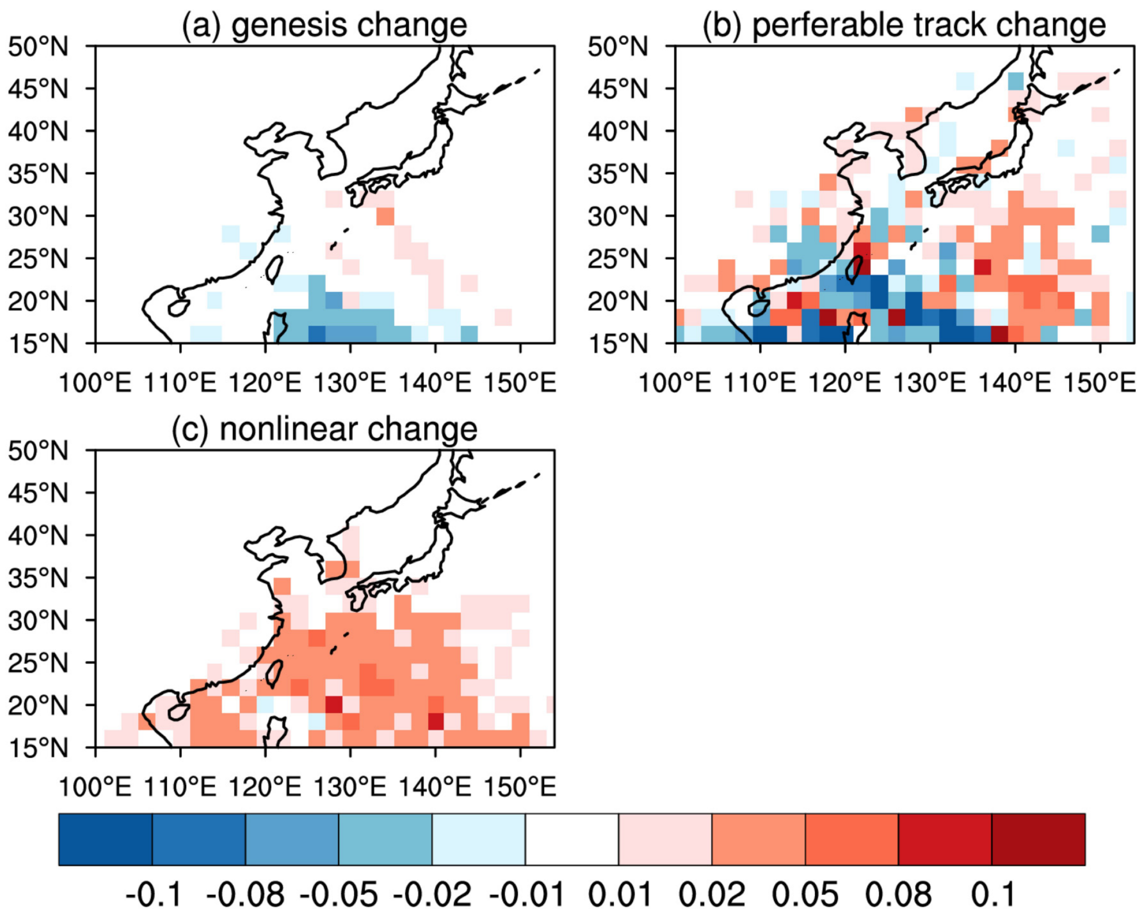

Fig. 13. Contributions of different factors to TC occurrence frequency changes for ensR over the WNP at the end of the 21st century (a) genesis frequency, (b) preferable track and (c) the nonlinear effect.

landfalls is projected to increase in most of the coastal provinces in China, except the Shanghai City with its small size of area coverage. The largest increase is found over Guangdong (0.27 yr^{-1}) followed by Zhejiang (0.18 yr^{-1}) and Fujian (0.13 yr^{-1}). When measured by percentage, the increase is largest in Shandong (111%), followed by Liaoning (100%) in the north, and Jiangsu (42%) in the central coastal regions. The total number of TC landfalls over China increases from 3.98 yr^{-1} in the present-day period to 4.69 yr^{-1} (18% increase) at the end of the century. The spread of the landfall number in most provinces is small during the two periods. The standard variation of the total landfall number over China is 0.67 yr^{-1} in the present and 0.73 yr^{-1} in the future, indicating a future increase in interannual variability.

Figure 15b presents the change of steering flow at the end of 21st century. This is characterized by two anti-cyclonic circulations with centers located over the northern part of China and the western WNP, centered at (115°E, 40°N) and (155°E, 25°N), respectively. Both circulation changes contribute to a prevailing onshore flow for most of the Chinese mainland (Fig. 15b), which favors TC landing and thus leads to the higher number of landfall TCs discussed above.

5. Summary and discussion

In this paper, the features of TC activity in current and future climate conditions over the WNP have been investigated by using an ensemble of RegCM4 simulations under the RCP4.5 pathway. Our main conclusions can be summarized as follows:

1) The model captures the general features of the observed TC activity, although with slightly underestimated number of genesis events and underestimated number of occurrences, as a result of shorter than observed tracks. The model underestimates very intense TCs, likely due to the coarse resolution of most models (e.g. Flato et al., 2013), but shows good performance for medium intensity and intense TCs. Overall, the simulations underestimate the number of landfall TCs in most coastal regions of China.

2) An increase in the TC genesis by ~16% averaged over the analysis region is projected by the end of the 21st century. The change of occurrence frequency shows a general increase, with a regional mean value of 10%. A slight northward shift of the TC occurrence in the future is also found.

3) The intensity of the TCs, in particular for the percentage of intense ones, is projected to increase over the WNP, consistent with previous studies (e.g. Seneviratne et al.,

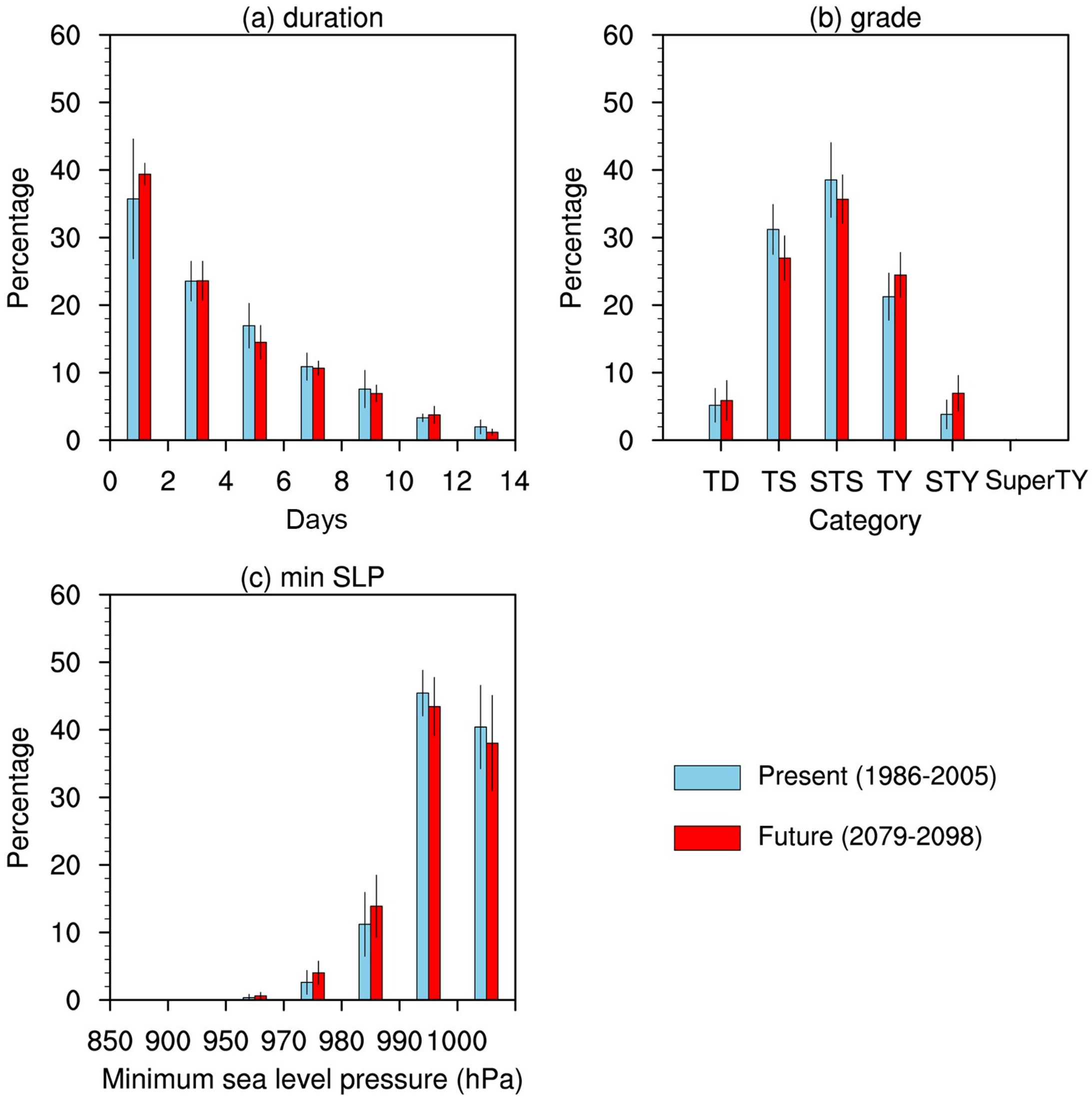

Fig. 14. Histograms of the percentages (%) of (a) TC duration, (b) different grades of TC and (c) minimum SLP for ensR for the present-day period of 1986–2005 (blue bars) and at the end of the 21st century (red bars). The vertical lines indicate one standard deviation of the five simulations.

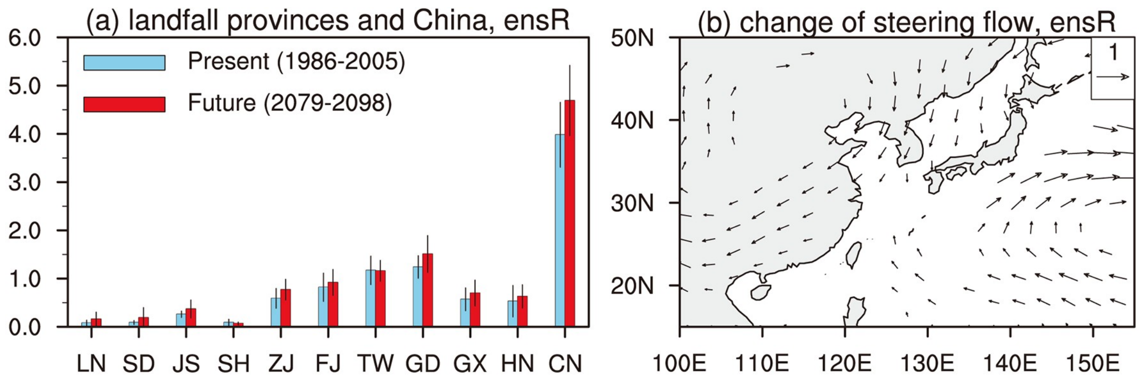

Fig. 15. (a) Histograms of annual mean number of landfall TCs (number per year) in the coastal provinces and whole of China for the present-day period of 1986–2005 and at the end of 21st century from ensR. (b) Changes of steering flow (vector; m s^{-1}) averaged from June to September for ensR at the end of 21st century, only shown those with p<0.05 (by the Student's t-test method). The vertical lines in (a) indicate one standard deviation of the five simulations.

2012). In addition, more TC landfalls over most coastal provinces of China are projected, indicating increased risks associated to TCs for coastal areas.

Large uncertainties still exist in the projection of future changes in TC activity. For example, our results showing increases in TC activity over the WNP are in line with the studies by Emanuel (2013, 2021), Vecchi et al. (2019) and Zhang and Wang (2017), but are different from those of Wang et al. (2017) and Wu et al. (2014). This is because the response of TC activity to global warming depends on a number of dynamical and thermodynamical processes acting on a range of spatial scales, and is strongly basin-dependent.

The spatial resolution of climate models is an important consideration for a better simulation and projection of TC activity. Although the 25 km grid spacing we used is the highest in conducting multiple RCM simulations over the WNP region, future simulations with higher resolution are needed, in particular for intense TCs (Murakami and Sugi, 2010; Jin et al., 2016; Wang et al., 2017). Further developments of the model itself are important, e.g. revised physics parameterizations (Reed and Jablonowski, 2011; Zhao et al., 2012; He and Posselt, 2015; Zhang and Wang, 2018) and dynamical cores (Camargo, 2013; Reed et al., 2015).

The model physics, in particular the convection scheme, plays an importan role in simulating the TCs (e.g. Murakami et al., 2012b; Diro et al., 2014; Fuentes-Franco et al., 2017; Zhang and Wang, 2018). With the continuous developments of RegCM4 and the implementation of new physical process schemes, further tests of new options [e.g. the Tiedtke (1989) convection scheme] need to be conducted to customize its performance in simulating TCs over the region. Furthermore, the domain used in the present study was designed as part of the CORDEX protocol for climate change studies over East Asia, and does not fully cover the full genesis region for TCs over the WNP basin. This calls for the use of targeted domains focusing on TC simulations over the region. Further diagnostics aimed at better understanding the complex mechanisms underlying model biases and changes are needed, as well as comparisons of different emission scenarios (Wang et al., 2017).

Last but not least, although we used the largest ensemble to date at 25 km grid scaling, the simulations employed in the present study used one RCM only and a limited number of driving GCMs. A more comprehensive assessment of future changes in TC activity over the region would thus require more comprehensive GCM-RCM model matrices with the newly released CMIP6 models and improved RCMs, which can be achieved under the framework of the CORDEX program. All these developments are currently under way and will be reported on in future studies.

Acknowledgements. The authors would like to thank the three anonymous reviewers for their valuable comments on this work. This research was jointly supported by the Strategic Priority Research Program of Chinese Academy of Sciences (Grant No. XDA20060401), the National Natural Science Foundation of China (Grant No. 41675103), and the Science and Technology Program of Yunnan (Grant No. 2018BC007). The authors acknowledge Geophysical Fluid Dynamics Laboratory for providing the TSTORMS (Detection and Diagnosis of Tropical Storms in High-Resolution Atmospheric Models) software code (available from https://www.gfdl.noaa.gov/tstorms/) to detect and track tropical cyclones in the present study.

REFERENCES

Au-Yeung, A. Y. M., and J. C. L. Chan, 2012: Potential use of a regional climate model in seasonal tropical cyclone activity predictions in the western North Pacific. *Climate Dyn.*, **39**, 783–794, https://doi.org/10.1007/s00382-011-1268-x.

Bengtsson, L., H. Böttger, and M. Kanamitsu, 1982: Simulation of hurricane-type vortices in a general circulation model. *Tellus*, **34**, 440–457, https://doi.org/10.3402/tellusa.v34i5.10830.

Bengtsson, L., M. Botzet, and M. Esch, 1995: Hurricane-type vortices in a general circulation model. *Tellus A*, **47**, 175–196, https://doi.org/10.3402/tellusa.v47i2.11500.

Bentsen, M., and Coauthors, 2013: The Norwegian Earth System Model, NorESM1-M–Part 1: Description and basic evaluation of the physical climate. *Geoscientific Model Development*, **6**, 687–720, https://doi.org/10.5194/gmd-6-687-2013.

Broccoli, A. J., and S. Manabe, 1990: Can existing climate models be used to study anthropogenic changes in tropical cyclone climate? Geophys *Res. Lett.*, **17**, 1917–1920, https://doi.org/10.1029/GL017i011p01917.

Camargo, S. J., 2013: Global and regional aspects of tropical cyclone activity in the CMIP5 models. *J. Climate*, **26**, 9880–9902, https://doi.org/10.1175/jcli-d-12-00549.1.

Camargo, S. J., and S. E. Zebiak, 2002: Improving the detection and tracking of tropical cyclones in atmospheric general circulation models. *Wea. Forecasting*, **17**, 1152–1162, https://doi.org/10.1175/1520-0434(2002)017<1152:itdato>2.0.co;2.

Chan, J. C. L., 2005: The physics of tropical cyclone motion. *Annual Review of Fluid Mechanics*, **37**, 99–128, https://doi.org/10.1146/annurev.fluid.37.061903.175702.

Chan, J. C. L., and M. Xu, 2009: Inter-annual and inter-decadal variations of landfalling tropical cyclones in East Asia. Part I: Time series analysis. *International Journal of Climatology*, **29**, 1285–1293, https://doi.org/10.1002/joc.1782.

Collins, W. J., and Coauthors, 2011: Development and evaluation of an Earth-System model-HadGEM2. *Geoscientific Model Development*, **4**, 1051–1075, https://doi.org/10.5194/gmd-4-1051-2011.

Dee, D. P., and Coauthors, 2011: The ERA-Interim reanalysis: Configuration and performance of the data assimilation system. *Quart. J. Roy. Meteor. Soc.*, **137**, 553–597, https://doi.org/10.1002/qj.828.

Diro, G. T., F. Giorgi, R. Fuentes-Franco, K. J. E. Walsh, G. Giuliani, and E. Coppola, 2014: Tropical cyclones in a regional climate change projection with RegCM4 over the CORDEX Central America domain. *Climatic Change*, **125**, 79–94, https://doi.org/10.1007/s10584-014-1155-7.

Emanuel, K. A., 1991: A scheme for representing cumulus convection in large-scale models. *J. Atmos. Sci.*, **48**, 2313–2335, https://doi.org/10.1175/1520-0469(1991)048<2313:asfrcc>2.0.co;2.

Emanuel, K. A., 2013: Downscaling CMIP5 climate models shows increased tropical cyclone activity over the 21st century. *Proceedings of the National Academy of Sciences of the United States of America*, **110**, 12219−12224, https://doi.org/10.1073/pnas.1301293110.

Emanuel, K. A., 2021: Response of global tropical cyclone activity to increasing CO_2: Results from downscaling CMIP6 models. *J. Climate*, **34**, 57−70, https://doi.org/10.1175/JCLI-D-20-0367.1.

Emanuel, K. A., and M. Živković-Rothman, 1999: Development and evaluation of a convection scheme for use in climate models. *J. Atmos. Sci.*, **56**, 1766−1782, https://doi.org/10.1175/1520-0469(1999)056<1766:daeoac>2.0.co;2.

Eyring, V., S. Bony, G. A. Meehl, C. A. Senior, B. Stevens, R. J. Stouffer, and K. E. Taylor, 2016: Overview of the Coupled Model Intercomparison Project Phase 6(CMIP6) experimental design and organization. *Geoscientific Model Development*, **9**, 1937−1958, https://doi.org/10.5194/gmd-9-1937-2016.

Flato, G., and Coauthors, 2013: Evaluation of climate models. *Climate Change 2013: The physical science basis. Contribution of Working Group I to the Fifth Assessment Report of the Intergovernmental Panel on Climate Change*, Stocker et al., Eds., Cambridge University Press, Cambridge, United Kingdom and New York, NY, USA, 741−866.

Fuentes-Franco, R., F. Giorgi, E. Coppola, and K. Zimmermann, 2017: Sensitivity of tropical cyclones to resolution, convection scheme and ocean flux parameterization over Eastern Tropical Pacific and Tropical North Atlantic Oceans in the RegCM4 model. *Climate Dyn.*, **49**, 547−561, https://doi.org/10.1007/s00382-016-3357-3.

Gao, X. J., Y. Shi, and F. Giorgi, 2016: Comparison of convective parameterizations in RegCM4 experiments over China with CLM as the land surface model. *Atmos. Ocean. Sci. Lett.*, **9**, 246−254, https://doi.org/10.1080/16742834.2016.1172938.

Gao, X. J., and Coauthors, 2017: Performance of RegCM4 over major river basins in China. *Adv. Atmos. Sci.*, **34**, 441−455, https://doi.org/10.1007/s00376-016-6179-7.

Gao, X. J., and Coauthors, 2018: Future changes in thermal comfort conditions over China based on multi-RegCM4 simulations. *Atmos. Ocean. Sci. Lett.*, **11**, 291−299, https://doi.org/10.1080/16742834.2018.1471578.

Gentry, M. S., and G. M. Lackmann, 2010: Sensitivity of simulated tropical cyclone structure and intensity to horizontal resolution. *Mon. Wea. Res.*, **138**, 688−704, https://doi.org/10.1175/2009MWR2976.1.

Giorgi, F., 2019: Thirty years of regional climate modeling: Where are we and where are we going next? J *Geophys. Res. Atmos.*, **124**, 5696−5723, https://doi.org/10.1029/2018jd030094.

Giorgi, F., M. R. Marinucci, G. T. Bates, and G. De Canio, 1993: Development of a second-generation regional climate model (REGCM2). Part II: Convective processes and assimilation of lateral boundary conditions. *Mon. Wea. Rev.*, **121**, 2814−2832, https://doi.org/10.1175/1520-0493(1993)121<2814:DOASGR>2.0.CO;2.

Giorgi, F., C. Jones, and G. R. Asrar, 2009: Addressing climate information needs at the regional level: The CORDEX framework. *WMO Bull.*, **58**, 175−183.

Giorgi, F., and Coauthors, 2012: RegCM4: Model description and preliminary tests over multiple CORDEX domains. *Climate Research*, **52**, 7−29, https://doi.org/10.3354/cr01018.

Gray, W. M., 1979: Meteorology over the tropical oceans. *Hurricanes: Their Formation, Structure and Likely Role in the Tropical Circulation*, D. B. Shaw, Eds., Royal Meteorological Society, 155−218.

Gutowski, W. J. Jr., and Coauthors, 2016: WCRP COordinated Regional Downscaling EXperiment (CORDEX): A diagnostic MIP for CMIP6. *Geoscientific Model Development*, **9**, 4087−4095, https://doi.org/10.5194/gmd-9-4087-2016.

Haarsma, R. J., J. F. B. Mitchell, and C. A. Senior, 1993: Tropical disturbances in a GCM. *Climate Dyn.*, **8**, 247−257, https://doi.org/10.1007/bf00198619.

Han, Z. Y., X. J. Gao, Y. Shi, J. Wu, M. L. Wang, and F. Giorgi, 2015: Development of Chinese high resolution land cover data for the RegCM4/CLM and its impact on regional climate simulation. *Journal of Glaciology and Geocryology*, **37**, 857−866, https://doi.org/10.7522/j.issn.1000-0240.2015.0095. (in Chinese with English abstract)

Hazeleger, W., and Coauthors, 2010: EC-Earth: A seamless earth-system prediction approach in action. *Bull. Amer. Meteor. Soc.*, **91**, 1357−1363, https://doi.org/10.1175/2010bams2877.1.

He, F., and D. J. Posselt, 2015: Impact of parameterized physical processes on simulated tropical cyclone characteristics in the community atmosphere model. *J. Climate*, **28**, 9857−9872, https://doi.org/10.1175/jcli-d-15-0255.1.

Holtslag, A. A. M., E. I. F. De Bruijn, and H. L. Pan, 1990: A high resolution air mass transformation model for short-range weather forecastiong. *Mon. Wea. Rev.*, **118**, 1561−1575, https://doi.org/10.1175/1520-0493(1990)118<1561:ahramt>2.0.co;2.

Huang, W.-R., and J. C. L. Chan, 2014: Dynamical downscaling forecasts of Western North Pacific tropical cyclone genesis and landfall. *Climate Dyn.*, **42**, 2227−2237, https://doi.org/10.1007/s00382-013-1747-3.

Iversen, T., and Coauthors, 2013: The Norwegian Earth System Model, NorESM1-M−Part 2: Climate response and scenario projections. *Geoscientific Model Development*, **6**, 389−415, https://doi.org/10.5194/gmd-6-389-2013.

Jiang, D. B., Z. P. Tian, and X. M. Liang, 2016: Reliability of climate models for China through the IPCC Third to Fifth Assessment Reports. *International Journal of Climatology*, **36**, 1114−1133, https://doi.org/10.1002/joc.4406.

Jin, C.-S., D.-H. Cha, D.-K. Lee, M.-S. Suh, S.-Y. Hong, H.-S. Kang, and C.-H. Ho, 2016: Evaluation of climatological tropical cyclone activity over the western North Pacific in the CORDEX-East Asia multi-RCM simulations. *Climate Dyn.*, **47**, 765−778, https://doi.org/10.1007/s00382-015-2869-6.

Jungclaus, J. H., and Coauthors, 2013: Characteristics of the ocean simulations in the Max Planck Institute Ocean Model (MPIOM) the ocean component of the MPI-Earth system model. *Journal of Advances in Modeling Earth Systems*, **5**, 422−446, https://doi.org/10.1002/jame.20023.

Kiehl, J. T., J. J. Hack, G. B. Bonan, B. A. Boville, D. L. Williamson, and P. J. Rasch, 1998: The National Center for Atmospheric Research community climate model: CCM3. *J. Climate*, **11**, 1131−1149, https://doi.org/10.1175/1520-0442(1998)011<1131:tncfar>2.0.co;2.

Knapp, K. R., M. C. Kruk, D. H. Levinson, H. J. Diamond, and C. J. Neumann, 2010: The International Best Track Archive for Climate Stewardship (IBTrACS): Unifying tropical cyclone data. *Bull. Amer. Meteor. Soc.*, **91**, 363−376, https://doi.org/10.1175/2009bams2755.1.

Kruk, M. C., K. R. Knapp, and D. H. Levinson, 2010: A technique for combining global tropical cyclone best track data. *J. Atmos. Ocean. Technol.*, **27**, 680–692, https://doi.org/10.1175/2009jtecha1267.1.

Lee, H., C. S. Jin, D. H. Cha, M. Lee, D. K. Lee, M. S. Suh, S. Y. Hong, and H. S. Kang, 2019: Future change in tropical cyclone activity over the Western North Pacific in CORDEX-East Asia multi-RCMs forced by HadGEM2-AO. *J. Climate*, **32**, 5053–5067, https://doi.org/10.1175/jcli-d-18-0575.1.

Li, R. C. Y., W. Zhou, C. M. Shun, and T. C. Lee, 2017: Change in destructiveness of landfalling tropical cyclones over China in recent decades. *J. Climate*, **30**, 3367–3379, https://doi.org/10.1175/jcli-d-16-0258.1.

Liang, J., C. G. Wang, and K. I. Hodges, 2017: Evaluation of tropical cyclones over the South China Sea simulated by the 12 km MetUM regional climate model. *Quart. J. Roy. Meteor. Soc.*, **143**, 1641–1656, https://doi.org/10.1002/qj.3035.

Lok, C. C. F., and J. C. L. Chan, 2018a: Changes of tropical cyclone landfalls in South China throughout the twenty-first century. *Climate Dyn.*, **51**, 2467–2483, https://doi.org/10.1007/s00382-017-4023-0.

Lok, C. C. F., and J. C. L. Chan, 2018b: Simulating seasonal tropical cyclone intensities at landfall along the South China coast. *Climate Dyn.*, **50**, 2661–2672, https://doi.org/10.1007/s00382-017-3762-2.

Manabe, S., J. L. Holloway Jr., and H. M. Stone, 1970: Tropical circulation in a time-integration of a global model of the atmosphere. *J. Atmos. Sci.*, **27**, 580–613, https://doi.org/10.1175/1520-0469(1970)027<0580:tciati>2.0.co;2.

Moss, R. H., and Coauthors, 2010: The next generation of scenarios for climate change research and assessment. *Nature*, **463**, 747–756, https://doi.org/10.1038/nature08823.

Murakami, H., and M. Sugi, 2010: Effect of model resolution on tropical cyclone climate projections. *SOLA*, **6**, 73–76, https://doi.org/10.2151/sola.2010-019.

Murakami, H., B. Wang, and A. Kitoh, 2011: Future change of western North Pacific typhoons: Projections by a 20-km-mesh global atmospheric model. *J. Climate*, **24**, 1154–1169, https://doi.org/10.1175/2010jcli3723.1.

Murakami, H., R. Mizuta, and E. Shindo, 2012a: Future changes in tropical cyclone activity projected by multi-physics and multi-SST ensemble experiments using the 60-km-mesh MRI-AGCM. *Climate Dyn.*, **39**, 2569–2584, https://doi.org/10.1007/s00382-011-1223-x.

Murakami, H., and Coauthors, 2012b: Future changes in tropical cyclone activity projected by the new high-resolution MRI-AGCM. *J. Climate*, **25**, 3237–3260, https://doi.org/10.1175/jcli-d-11-00415.1.

Murakami, H., M. Sugi, and A. Kitoh, 2013a: Future changes in tropical cyclone activity in the North Indian Ocean projected by high-resolution MRI-AGCMs. *Climate Dyn.*, **40**, 1949–1968, https://doi.org/10.1007/s00382-012-1407-z.

Murakami, H., B. Wang, T. Li, and A. Kitoh, 2013b: Projected increase in tropical cyclones near Hawaii. *Nature Climate Change*, **3**, 749–754, https://doi.org/10.1038/nclimate1890.

Oleson, K. W., and Coauthors, 2008: Improvements to the Community Land Model and their impact on the hydrological cycle. *J. Geophys. Res. Biogeosci.*, **113**, https://doi.org/10.1029/2007jg000563.

Oouchi, K., J. Yoshimura, H. Yoshimura, R. Mizuta, S. Kusunoki, and A. Noda, 2006: Tropical cyclone climatology in a global-warming climate as simulated in a 20 km-mesh global atmospheric model: Frequency and wind intensity analyses. *J. Meteor. Soc. Japan*, **84**, 259–276, https://doi.org/10.2151/jmsj.84.259.

Pal, J. S., E. E. Small, and E. A. B. Eltahir, 2000: Simulation of regional-scale water and energy budgets: Representation of subgrid cloud and precipitation processes within RegCM. *J. Geophys. Res. Atmos.*, **105**, 29579–29594, https://doi.org/10.1029/2000jd900415.

Pal, J. S., and Coauthors, 2007: Regional climate modeling for the developing world: The ICTP RegCM3 and RegCNET. *Bull. Amer. Meteor. Soc.*, **88**, 1395–1410, https://doi.org/10.1175/bams-88-9-1395.

Phan-Van, T., L. Trinh-Tuan, H. Bui-Hoang, and C. Kieu, 2015: Seasonal forecasting of tropical cyclone activity in the coastal region of Vietnam using RegCM4.2. *Climate Researc*, **62**, 115–129, https://doi.org/10.3354/cr01267.

Reed, K. A., and C. Jablonowski, 2011: Assessing the uncertainty in tropical cyclone simulations in NCAR's Community Atmosphere Model. *Journal of Advances in Modeling Earth Systems*, **3**, M08002, https://doi.org/10.1029/2011ms000076.

Reed, K. A., J. T. Bacmeister, N. A. Rosenbloom, M. F. Wehner, S. C. Bates, P. H. Lauritzen, J. E. Truesdale, and C. Hannay, 2015: Impact of the dynamical core on the direct simulation of tropical cyclones in a high-resolution global model. *Geophys. Res. Lett.*, **42**, 3603–3608, https://doi.org/10.1002/2015gl063974.

Rotstayn, L. D., and Coauthors, 2010: Improved simulation of Australian climate and ENSO-related rainfall variability in a global climate model with an interactive aerosol treatment. *International Journal of Climatology*, **30**, 1067–1088, https://doi.org/10.1002/joc.1952.

Seneviratne, S. I., and Coauthors, 2012: Changes in climate extremes and their impacts on the natural physical environment. *Managing the Risks of Extreme Events and Disasters to Advance Climate Change Adaptation. A Special Report of Working Groups I and II of the Intergovernmental Panel on Climate Change (IPCC)*, Field et al., Eds., Cambridge University Press, Cambridge, UK, and New York, NY, USA, 109–230.

Shen, W. Q., J. P. Tang, Y. Wang, S. Y. Wang, and X. R. Niu, 2017: Evaluation of WRF model simulations of tropical cyclones in the western North Pacific over the CORDEX East Asia domain. *Climate Dyn.*, **48**, 2419–2435, https://doi.org/10.1007/s00382-016-3213-5.

Stevens, B., and Coauthors, 2013: Atmospheric component of the MPI-M Earth System Model: ECHAM6. *Journal of Advances in Modeling Earth Systems*, **5**, 146–172, https://doi.org/10.1002/jame.20015.

Taylor, K. E., R. J. Stouffer, and G. A. Meehl, 2012: An overview of CMIP5 and the experiment design. *Bull. Amer. Meteor. Soc.*, **93**, 485–498, https://doi.org/10.1175/bams-d-11-00094.1.

Tiedtke, M., 1989: A comprehensive mass flux scheme for cumulus parameterization in large-scale models. *Mon. Wea. Rev.*, **117**, 1779–1800, https://doi.org/10.1175/1520-0493(1989)117<1779:acmfsf>2.0.co;2.

Vecchi, G. A., and Coauthors, 2019: Tropical cyclone sensitivities to CO_2 doubling: Roles of atmospheric resolution, synoptic variability and background climate changes. *Clim. Dyn.*,

53, 5999–6033, https://doi.org/10.1007/s00382-019-04913-y.

Walsh, K. J. E., M. Fiorino, C. W. Landsea, and K. L. McInnes, 2007: Objectively determined resolution-dependent threshold criteria for the detection of tropical cyclones in climate models and reanalyses. *J. Climate*, **20**, 2307–2314, https://doi.org/10.1175/jcli4074.1.

Wang, C. G., J. Liang, and K. I. Hodges, 2017: Projections of tropical cyclones affecting Vietnam under climate change: Downscaled HadGEM2-ES using PRECIS 2.1. *Quart. J. Roy. Meteor. Soc.*, **143**, 1844–1859, https://doi.org/10.1002/qj.3046.

Wang, Y. J., S. S. Wen, X. C. Li, F. Thomas, B. D. Su, R. Wang, and T. Jiang, 2016: Spatiotemporal distributions of influential tropical cyclones and associated economic losses in China in 1984-2015. *Natural Hazards*, **84**, 2009–2030, https://doi.org/10.1007/s11069-016-2531-6.

Wu, J., and X. J. Gao, 2020: Present day bias and future change signal of temperature over China in a series of multi-GCM driven RCM simulations. *Climate Dyn.*, **54**, 1113–1130, https://doi.org/10.1007/s00382-019-05047-x.

Wu, L., and Coauthors, 2014: Simulations of the present and late-twenty-first-century western North Pacific tropical cyclone activity using a regional model. *J. Climate*, **27**, 3405–3424, https://doi.org/10.1175/jcli-d-12-00830.1.

Wu, L. G., B. Wang, and S. Q. Geng, 2005: Growing typhoon influence on East Asia. *Geophys. Res. Lett.*, **32**, L18703, https://doi.org/10.1029/2005gl022937.

Yokoi, S., Y. N. Takayabu, and H. Murakami, 2013: Attribution of projected future changes in tropical cyclone passage frequency over the western North Pacific. *J. Climate*, **26**, 4096–4111, https://doi.org/10.1175/jcli-d-12-00218.1.

Zeng, X. B., and A. Beljaars, 2005: A prognostic scheme of sea surface skin temperature for modeling and data assimilation. *Geophys. Res. Lett.*, **32**, L14605, https://doi.org/10.1029/2005GL023030.

Zhang, C. X., and Y. Q. Wang, 2017: Projected future changes of tropical cyclone activity over the western North and South Pacific in a 20-km-mesh regional climate model. *J. Climate*, **30**, 5923–5941, https://doi.org/10.1175/jcli-d-16-0597.1.

Zhang, C. X., and Y. Q. Wang, 2018: Why is the simulated climatology of tropical cyclones so sensitive to the choice of cumulus parameterization scheme in the WRF model? *Climate Dyn.*, **51**, 3613–3633, https://doi.org/10.1007/s00382-018-4099-1.

Zhang, Q., L. G. Wu, and Q. G. Liu, 2009: Tropical cyclone damages in China 1983-2006. *Bull. Amer. Meteor. Soc.*, **90**, 489–496, https://doi.org/10.1175/2008bams2631.1.

Zhao, M., I. M. Held, S.-J. Lin, and G. A. Vecchi, 2009: Simulations of global hurricane climatology, interannual variability, and response to global warming using a 50-km resolution GCM. *J. Climate*, **22**, 6653–6678, https://doi.org/10.1175/2009jcli3049.1.

Zhao, M., I. M. Held, and S.-J. Lin, 2012: Some counterintuitive dependencies of tropical cyclone frequency on parameters in a GCM. *J. Atmos. Sci.*, **69**, 2272–2283, https://doi.org/10.1175/jas-d-11-0238.1.